# Effective in-plane elastic moduli of quasi-random spatially irregular hexagonal lattices


## Abstract

An analytical framework is developed for predicting the effective in-plane elastic moduli (longitudinal and transverse Young's modulus, Poisson's ratios and shear modulus) of irregular hexagonal lattices with generalized form of spatially random structural geometry. On the basis of a mechanics based bottom-up multi-step approach, computationally efficient closed-form formulae are derived in this article. As a special case when there is no irregularity, the derived analytical expressions reduce to the respective well known formulae of regular honeycombs available in literature. Previous analytical investigations include the derivation of effective in-plane elastic moduli for hexagonal lattices with spatially random variation of cell angles, which is a special case of the generalized form of irregularity in material and structural attributes considered in this paper. The present study also includes development of a highly generalized finite element code for obtaining equivalent elastic properties of random lattices, which is employed to validate the proposed analytical formulae. The statistical results of elastic moduli obtained using the developed analytical expressions and using direct finite element simulations are noticed to be in good agreement affirming the accuracy and validity of the proposed analytical framework. All the in-plane elastic moduli are found to be significantly influenced by spatially random irregularity resulting in a decrease of the mean values for the two Young's moduli and two Poisson's ratios, while an increase of the mean value for the shear modulus.



*Keywords:* Hexagonal lattice; Spatial irregularity; In-plane elastic moduli; Cellular structure; Honeycomb, Quasi-periodicity


## 1. Introduction

Hexagonal lattices/ lattice-like structural forms are present as materials and structures in abundance across various length-scales (nano, micro and macro) within natural systems and artificial products, as shown in figure 1 (Gibson and Ashby, 1999). Such structures have received considerable attention in last few decades as an advanced material because of the capability to meet high performance application-specific demands in various critically desirable parameters such as specific strength

and stiffness, crushing resistance, fatigue strength, acoustic properties, shock absorption properties, electro-mechanical properties, corrosion and fire resistance (Gibson and Ashby, 1999). The application of honeycomb cores for lightweight sandwich structures is an active area of research (Mukhopadhyay and Adhikari, 2016c; Yongqiang and Zhiqiang, 2008; Zenkert, 1995). Honeycomb grill is commonly used to reduce noise and facilitate smooth airflow in computer fans. An in-depth understanding of the structural behaviour of such hexagonal lattices is useful in emerging research fields of nano-materials like Graphene and Boron Nitride, which are often idealized as hexagonal periodic structures (Liu et al., 2012; Mukhopadhyay et al., 2016a; Pantano et al., 2004).

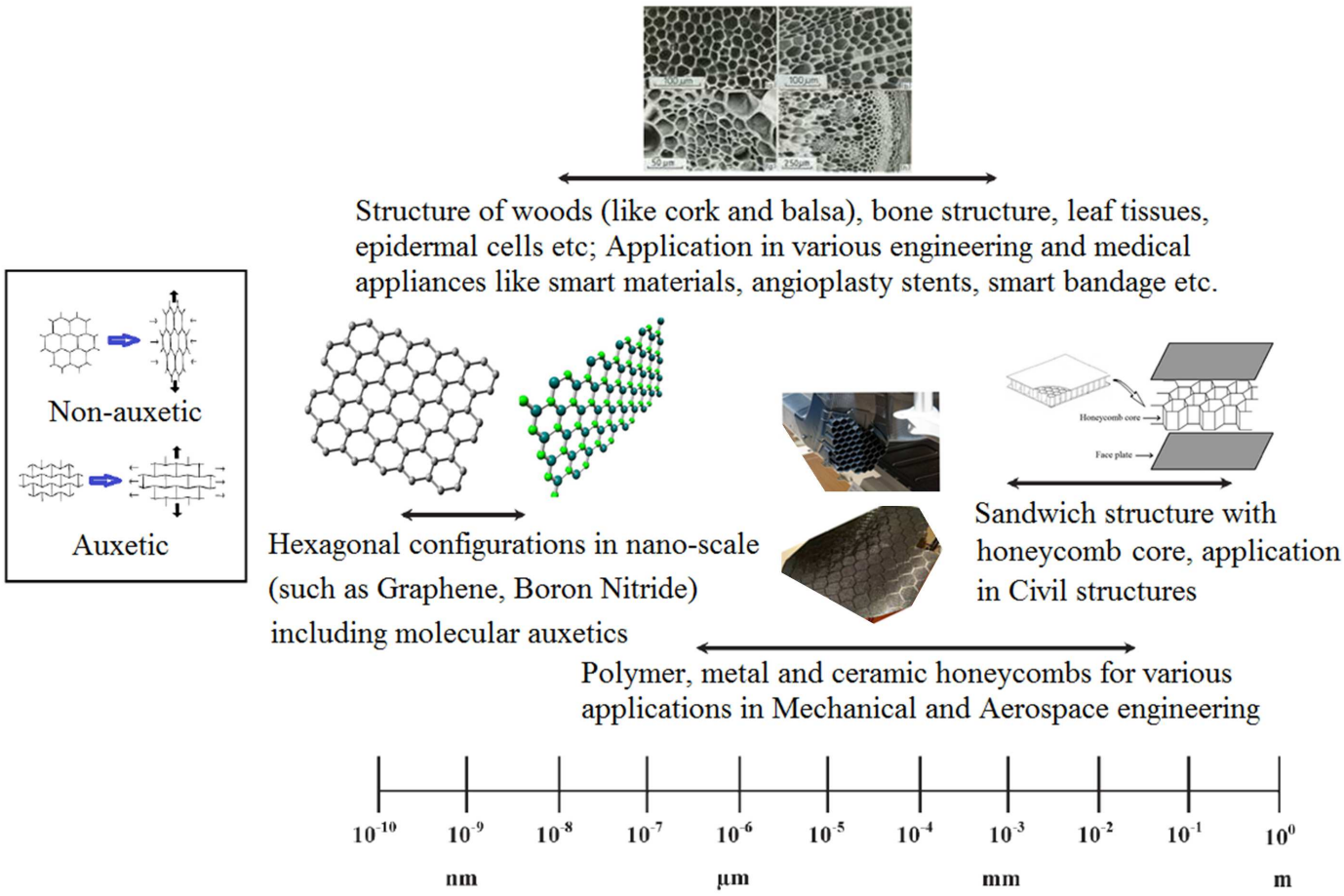


Figure 1: Occurrence and application of hexagonal lattices across the length scales

To eliminate the need of a detailed finite element modelling for hexagonal lattices/ honeycombs as a part of another complex structural system (host structure such as a sandwich panel), such lattices are generally modelled as a continuous solid medium with equivalent elastic moduli throughout the domain. For example, the effective elastic properties of the honeycomb-core are required to characterize the static and dynamic response of the sandwich panels such as deflection, natural frequency etc.

Estimation of effective elastic properties is quite common in the literature of mechanical sciences (Michel et al., 1999; Tang and Felicelli, 2015; Vilchevskaya and Sevostianov, 2015). A similar approach is followed to evaluate the effective material properties of different nano-structures having hexagonal configurations (Mukhopadhyay et al., 2016a). It is a common practice to consider a representative unit cell to model various other periodic structures (Javid et al., 2016). Extensive research has been conducted so far to predict effective elastic properties of regular hexagonal lattices without any form of irregularity (El-Sayed et al., 1979; Gibson and Ashby, 1999; Goswami, 2006; Malek and Gibson, 2015; Zhang and Ashby, 1992). Other crucial research areas concerning different responses related to honeycombs include crushing behaviour, low velocity impact, buckling analysis and wave propagation through lattices (Gonella and Ruzzene, 2008a,b; Hu and Yu, 2013; Jang and Kyriakides, 2015; Jimenez and Triantafyllidis, 2013; Klintworth and Stronge, 1988; Liu et al., 2016; Schaeffer and Ruzzene, 2015; Wilbert et al., 2011; Zschernack et al., 2016). A substantial amount of scientific literature is available dealing with perfectly periodic hexagonal auxetic lattices (Critchley et al., 2013; Evans and Alderson, 2000). Recently theoretical formulations have been presented for equivalent elastic properties of periodic asymmetrical honeycomb (Chen and Yang, 2011). Tailorable elastic properties of hierarchical honeycombs and spiderweb honeycombs have also been reported (Ajdari et al., 2012; Mousanezhad et al., 2015). Analysis of two dimensional hexagonal lattices/honeycombs, as presented in the above literature review, are based on an unit cell approach, which can be applied only for perfectly periodic lattice forms.

The major limitation of the aforementioned unit cell based approach is that it cannot be used to analyse a system with spatial irregularity. Spatial irregularity/variability in lattices is practically inevitable; it may occur due to structural defects, manufacturing uncertainty, variation in temperature, micro-structural variability and pre-stressing. Moreover, development of novel metamaterials (Mukhopadhyay and Adhikari, 2017; Srivastava, 2016) having hexagonal micro-structures may involve spatially varying structural and material attributes. To consider the effect of irregularity in cellular lattices, voronoi honeycombs are found to be considered in the literature (Li et al., 2005; Zhu et al., 2001, 2006). Dynamic crushing of honeycombs with irregularity in cell wall thickness and cell shapes have been investigated (Li et al., 2007). Triantafyllidis and Schraad (1998) have studied the failure surface of aluminium honeycombs for general inplane loading considering micro-structural imperfections. Papka and Kyriakides (1994, 1998) and Jang and Kyriakides (2015) have reported numerical and experimental study of honeycomb crushing and buckling behaviour accounting geometrical imperfections, such as over/ under expanded cells and variation in length of bond line. The effect due

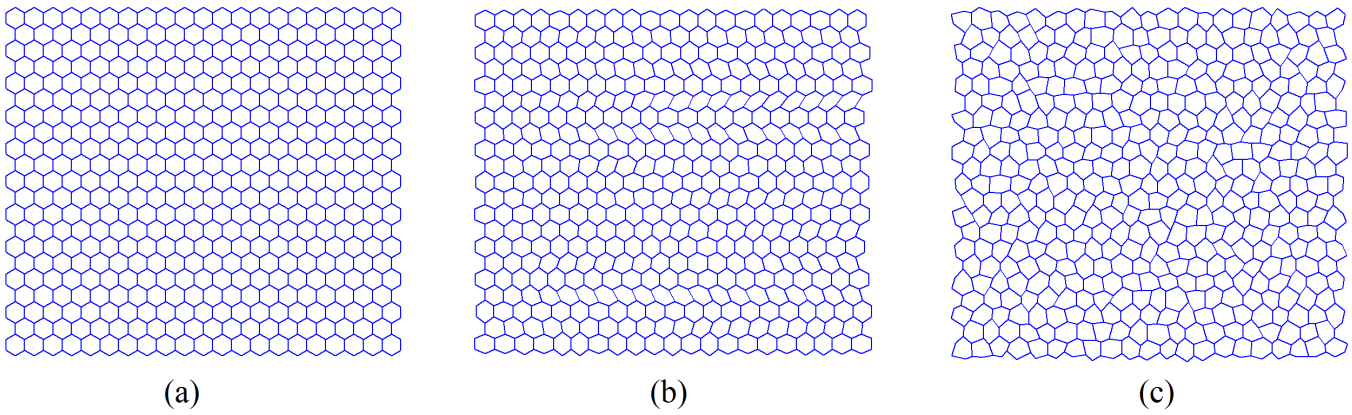


Figure 2: Typical representation for (a) a regular hexagonal lattice (b) an irregular hexagonal lattice with spatially random cell angle (c) an irregular hexagonal lattice with generalized form of spatially varying structural randomness

to defects on regular as well as voronoi honeycombs and the effect of manufacturing uncertainty on auxetic honeycomb have been reported by Ajdari et al. (2008) and Liu et al. (2014), respectively. Though the above mentioned studies substantially investigate the effect of irregularities based on limited number of expensive samples, there is a further need to extend these works following a more realistic and robust probabilistic framework for spatially random imperfections/irregularities in order to develop appropriate uncertainty quantification models. For voronoi honeycombs, the shape of all the irregular cells may not be necessarily hexagonal that violates the presumption of hexagonal cell structure. A thorough review of the literature on hexagonal lattices/ honeycomb dealing with different forms of structural irregularity reveals that the investigations are commonly based on either expensive finite element (FE) simulations or experimental investigations. As experimental investigations are expensive and time consuming, it is practically not feasible to quantify the effect of random irregularities in lattice structures by testing huge numbers of samples. In the finite element approach, a small change in the geometry of a constituent cell may require a completely new mesh generation. For dynamic and quasi-static analysis, separate finite element modelling of the honeycomb core in a sandwich structure may increase the degrees of freedom for the entire system up to such an extent that makes the overall process unmanageably complex and prohibitively expensive for simulation. In case of uncertainty quantification using a Monte Carlo based approach, the problem aggravates as a large number of expensive finite element simulations are needed to be carried out (Dey et al., 2017a,b, 2016a,b,c,d; Hurtado and Barbat, 1998; Mahata et al., 2016; Mukhopadhyay, 2017; Mukhopadhyay et al., 2015, 2016b,c). Application of surrogate based approaches to achieve computational efficiency, as adopted in many of these papers, does not make the analysis physically insightful and this approach

often suffer from lack of confidence in the predicted results. Moreover, surrogate based approaches may not perform well in case of high non-linearity in the model and high dimensional input parameter space, which becomes a crucial factor in analysing spatially irregular lattices. Besides that, for identifying application-specific lattice microstructure of novel materials following an inverse approach based on optimization may also require large number of iterations. Moreover, a large scale numerical simulation to quantify the effect of irregularity in cellular lattices may not necessarily yield proper understanding of the underlying physics of the system. An analytical approach for this purpose could be a simple, efficient, yet an insightful alternative. Recently an analytical framework has been reported for in-plane elastic moduli of hexagonal honeycombs with spatially varying cell angles as shown in figure 2(b) (Mukhopadhyay and Adhikari, 2016a,b). However, this model of irregularity is of limited practical resemblance and can be regarded as a random distribution of over and under expanded cells only. Thus there exists a strong rationale to develop realistic analytical formulations for a generalized spatially random irregularity model (as shown in figure 2(c)), wherein the irregular cells are randomly disordered following a generalized pattern, but they still maintain a hexagonal structural configuration. Moreover, spatially random variation of intrinsic elastic modulus is also an important factor for investigation in this regard.

In the present paper, we have developed an analytical model for generalized spatial randomness in structural and material attributes (individual and compound effects) to quantify the effect of irregularity in the effective in-plane elastic properties. The previously developed formulation for in-plane elastic moduli dealing with variation in cell angle only (Mukhopadhyay and Adhikari, 2016a,b) can be treated as a special case of the present analytical model. The closed-form expressions developed here can be a computationally efficient and less-tedious alternative to the conventional expensive finite element simulation approach for various applications. This paper is organized hereafter as follows. The description of the underlying concepts of the proposed bottom-up approach including detailed explanation of the definition for degree of irregularity are described in section 2. Analytical derivation of the expressions for the five in-plane elastic moduli is given in section 3. Validation of the closed-form expressions for in-plane elastic moduli with the results of direct finite element simulation and detailed results with appropriate discussions on the effect of spatially random irregularity is furnished in section 4. Summary of the results and discussion on the perspective of this paper is provided in section 5. Finally, section 6 presents the conclusion and prospective future works on the basis of the concepts developed in this paper.

## 2. Spatially random irregularity in hexagonal lattices

### *2.1. The concept of a representative unit cell element (RUCE)*

The aim of this work is to develop an analytical framework for deriving closed-form expressions of effective in-plane elastic moduli for spatially irregular hexagonal lattices, wherein the structural units are different in geometry along a two-dimensional plane; but they do maintain a particular shape. One structural unit may be considered as shown in figure 3(b) and the entire lattice structure shown in figure 3(a) is basically a tessellation of the shape shown in figure 3(b) with different values of the lengths of the three members and their orientations. Thus such repetition of the representative units can be referred as quasi-periodicity. The underlying philosophy of the proposed idea is that the entire irregular hexagonal lattice structure consists of several representative unit cell elements (RUCE) at the elementary level as shown in figure 3(a). Each of the RUCEs possess different individual elastic moduli depending on its structural geometry and intrinsic material properties (i.e. $l_1$, $l_2$, $l_3$, $\alpha$, $\beta$, $\gamma$, $E_s$ are different for the RUCEs in the present analysis; refer to figure 5 for the symbols). The effect of irregularity in material and geometric attributes are accounted in the elementary local level first by analysing the RUCEs and then the effect of such irregularity is propagated to the global scale (equivalent in-plane properties of the entire irregular lattice structure). This is achieved by following a multi-scale and multi-stage framework as described in figure 4. The closed-form formulae for five in-plane elastic moduli of a single RUCE are derived as a function of their respective material and geometric attributes. Thus the formulae developed for a single RUCE is effectively capable of expressing the equivalent material properties at local scale. The RUCEs are idealized further in this stage on the basis of the adopted assembling scheme. Subsequently, using the formulae for a single idealized RUCE, the expressions for effective elastic moduli of the entire irregular lattice are derived based on the basic principles of mechanics along with the equilibrium and deformation compatibility conditions following a multi-stage approach.

The analytical framework of deriving closed-form formulae for elastic moduli of the entire irregular lattice structure consists of the following four stages: selection of appropriate RUCE (for capturing local behaviour) and adoption of a proper idealization scheme (for propagating the local attributes to global level); derivation of expressions for in-plane elastic moduli of a generalized RUCE in terms of material and geometric properties; derivation of equivalent elastic moduli for each strip (refer to figure 4) in terms of the equivalent material properties of individual constituent RUCEs of that particular strip and finally, derivation of the in-plane elastic moduli of the entire irregular lattice in terms of the equivalent elastic moduli of the constituent strips. Thus, the expressions for equivalent

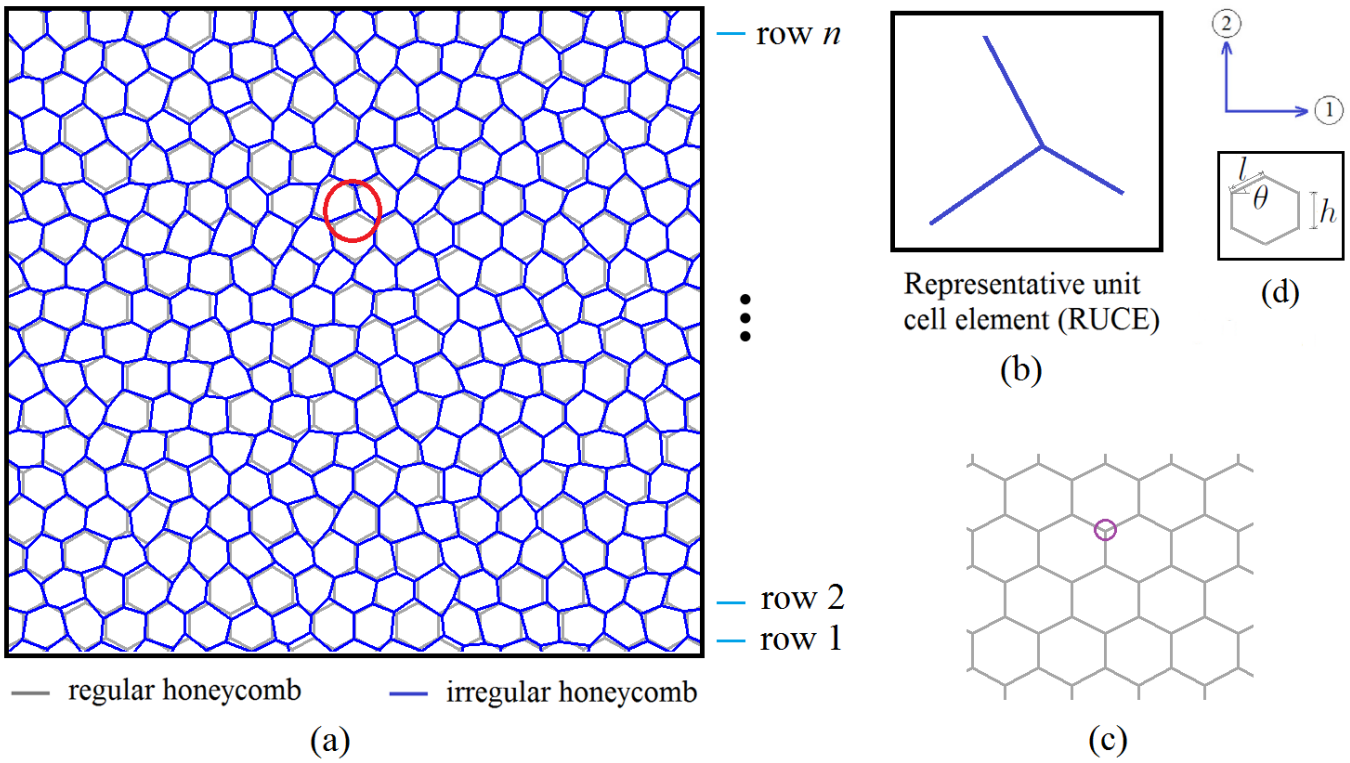


Figure 3: (a) Typical representation of an irregular honeycomb (b) Representative unit cell element (RUCE) (c) Illustration to define degree of irregularity (d) Unit cell considered for regular hexagonal lattice by Gibson and Ashby (1999)

elastic moduli of the entire irregular structure are necessarily developed in terms of the material and geometric attributes at elementary local level.

In the proposed analytical approach, each representative units (structural elements) of the lattice are considered to possess random structural and material attributes, instead of considering homogenized properties like a conventional unit cell that remains constant throughout the entire domain. In the traditional approach, typically one unit cell is considered for the purpose of analysis. It is assumed that a single such unit cell represents the entire analysis domain. However, this way of analysis is invalid for stochastic systems having spatially varying structural and material properties, because the constituent unit cells are not identical. Through the introduction of the concept of RUCE, the random structural attributes along the spatial location are accounted for analysing such irregular systems. In the present bottom-up framework, the RUCEs are chosen from the viewpoint of the adopted discretization scheme (refer figure 4) so that, being the smallest possible elementary units, they can be used to capture the local material and geometric attributes effectively. Another crucial factor is that the RUCEs should reasonably facilitate to assemble their individual local properties to the 'strip' level first, and thereby to the 'global' level considering idealized blocks based on principles of mechanics.

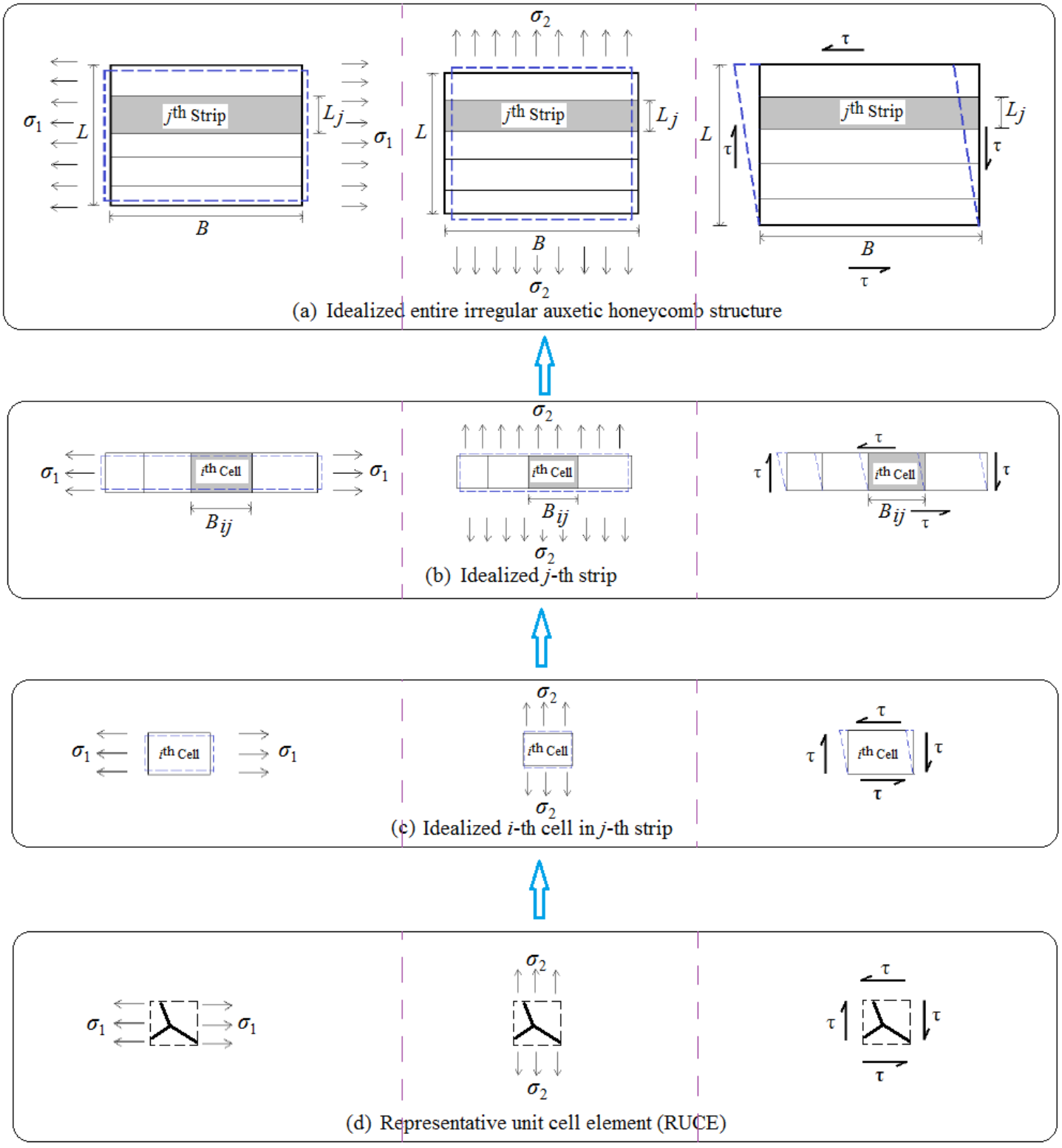


Figure 4: Idealization of RUCE and proposed bottom-up approach for propagation of the effect of irregularity from an elementary level to the global level

Here the RUCEs are basically the representative elementary building blocks of the entire irregular hexagonal lattice. For this reason, the word 'element' is used in the nomenclature 'RUCE'. It is com-

mon in the literature of honeycombs and other lattice structures (Gibson and Ashby (1999)) to use the phrase 'unit cell' for analysing regular lattices, where the structure of the unit cell repeats in a plane. However, the present analysis deals with irregular lattice that consists of several such unit cells, each of them having different structural geometry (though there exists a particular pattern in the structural geometry). Thus each of the unit cells have different equivalent properties in case of such irregular lattice. Local elastic properties of the RUCEs are represented as a function of structural and material irregularity $Z_U(\omega)$, where the parameter $\omega$ is used to denote the random structural geometry/ irregularity. Here $Z$ and $U$ denote a particular in-plane elastic modulus and representative unit (RUCE), respectively. To emphasize the fact that each 'unit cell' has different property in the present analysis, the word 'representative' is used. To portray all the above three characteristics simultaneously ('representative', 'unit cell' and 'element') the word RUCE (representative unit cell element) is chosen in context to the proposed analysis of irregular lattices.

It is noteworthy that effectively three different loading directions are required to be analysed for derivation of the expressions for five in-plane elastic moduli (refer figure 4). Stress $\sigma_1$ is applied in direction-1 for longitudinal Young's modulus ($E_1$) and Poisson's ratio $\nu_{12}$, while for analysing transverse Young's modulus ($E_2$) and Poisson's ratio $\nu_{21}$, stress $\sigma_2$ is applied in direction-2. Shear stress $\tau$ is applied to obtain the expression of shear modulus ($G_{12}$). The directions used are indicated in figure 3. The notations used in the proposed multi-stage analysis for deriving the formulae of different elastic moduli throughout this article are as follows, $Z_U$: elastic moduli of a single RUCE; $Z_U^I$: elastic moduli of a single idealized RUCE; $\hat{Z}$: effective elastic moduli of a single strip; $Z_{eq}$: equivalent elastic moduli of the entire irregular lattice, where $Z$ represents a particular elastic modulus. For example, $E_{1U}$ denotes the equivalent Young's modulus in direction-1 for a single RUCE. The subscripts $i$ and $j$ ($i = 1, 2, 3, ..., m$ and $j = 1, 2, 3, ..., n$) are used to indicate the location of the RUCE or a particular strip under consideration. In the present analysis, the entire irregular lattice is assumed to have $m$ and $n$ number of RUCEs in direction-1 and direction-2, respectively. Thus, to denote a particular parameter, the subscript of $ij$ is used when a RUCE (/idealized RUCE) is referred corresponding to a position of $i^{th}$ column and $j^{th}$ row ($Z_{ij}$), while subscript $j$ is used to refer a particular strip corresponding to $j^{th}$ row ($Z_j$). The formulae developed are applicable for both compressive as well as tensile stresses.

*2.2. Definition of the degree of irregularity*

To put the results into a proper context, a mathematically consistent and physically relevant measure of irregularity in a lattice structure is necessary. The effect of irregularity on the effective in-plane material properties of the entire lattice is dependent on the degree of disorder in the structural geometry with respect to the regular configuration as shown in figure 3(a). To de fine the degree of irregularity, it is assumed that each connecting node of the lattice moves randomly within a certain radius ($r_d$) around the respective node corresponding to the regular deterministic configuration as described in figure 3(c). For physically realistic variabilities, it is considered that a given node do not cross a neighbouring node, that is

$$r_d < \min\left(\frac{h}{2}, \frac{l}{2}, l\cos\theta\right) \tag{1}$$

In each realization of the Monte Carlo simulation, all the nodes of the lattice move simultaneously to new random locations within the specified circular bounds. Thus, the degree of irregularity ($r$) is defined as a non-dimensional ratio of the area of the circle and the area of one regular hexagonal unit as

$$r = \frac{\pi r_d^2 \times 100}{2l\cos\theta(h + l\sin\theta)} \tag{2}$$

The notations used in the above expression for the degree of irregularity are explained in figure 3(d). The degree of irregularity ($r$) has been expressed as percentage values for presenting the results in this paper. The term 'quasi' is used to denote the form of structural irregularity considered in this study because of the fact that even though the type of irregularity is quite general in nature, the lattice still maintains a hexagonal cellular configuration following a practical and controlled variability depending on the value of $r$.

## 3. Analytical derivation of the expressions for in-plane elastic moduli

The derivation of closed-form expressions for the five in-plane elastic moduli of irregular lattices as a function of its material and geometric attributes is discussed in this section. The expressions for the elastic moduli of a single idealized RUCE are obtained first and thereby the final closed-form formulae for the entire irregular lattice are derived based on the expressions of equivalent material properties for a single idealized RUCE.

*3.1. Longitudinal Young's modulus*

*3.1.1. Longitudinal Young's modulus for an idealized RUCE*

Stress $\sigma_1$ is applied in direction-1 (refer figure 5) for deriving the expression of longitudinal Young's modulus for a single RUCE ($E_{1U}$). From the condition of vertical equilibrium the free-body diagram as shown in figure 5(c), it can be concluded that the vertical forces acting on points A and B should

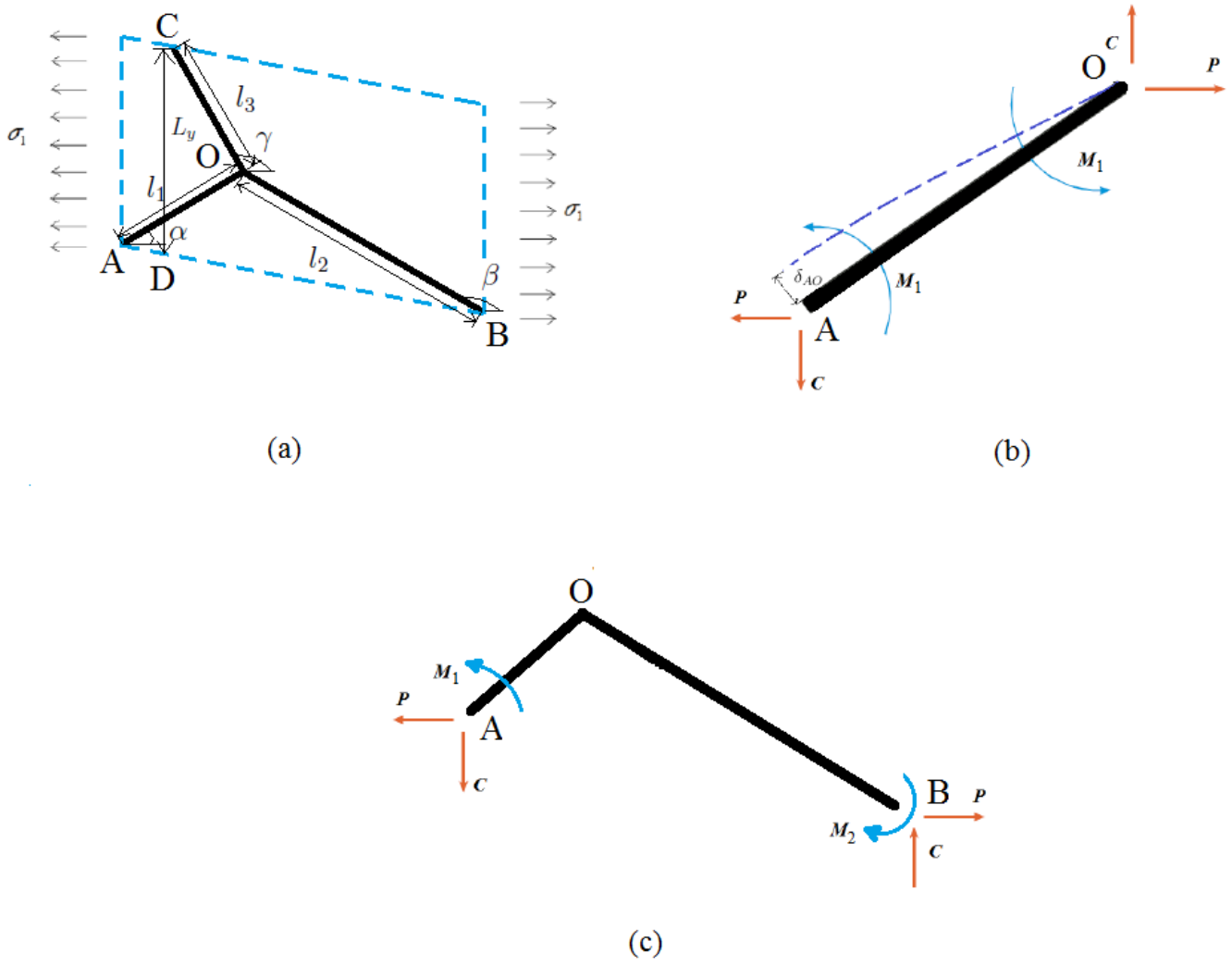


Figure 5: RUCE and free-body diagram for the proposed analysis of $E_{1U}$

be of equal magnitude and opposite sign. The horizontal forces acting on points A and B can be expressed as $P = \sigma_1 L_y b$, where $L_y$ represents the length CD and $b$ is the height of honeycomb sheet (dimension perpendicular to the 1-2 plane). $M_1$ and $M_2$ can be expressed as

$$M_1 = \frac{1}{2}(Pl_1 \sin\alpha - Cl_1 \cos\alpha) \tag{3}$$

$$M_2 = \frac{1}{2}(Pl_2 \sin\beta - Cl_2 \cos\beta) \tag{4}$$

Considering the rotational equilibrium of the free-body diagram presented in figure 5(c), the expression for $C$ can be obtained as

$$C = P\left(\frac{l_1 \sin\alpha - l_2 \sin\beta}{l_1 \cos\alpha - l_2 \cos\beta}\right) \tag{5}$$

The horizontal deflection of point A with respect to point O ($\delta^h_{AO}$) consists of the deflection due to force $P$ and the force $C$ (Roark and Young, 1976)

$$\delta^h_{AO} = \left(\frac{P l_1^3 \sin\alpha}{12 E_s I} - \frac{C l_1^3 \cos\alpha}{12 E_s I}\right) \sin\alpha \tag{6}$$

where the first and second terms in the bracket represents the deflection of point A with respect to point O in the direction perpendicular to AO due to forces $P$ and $C$ respectively. The superscript $h$ is used to represent horizontal direction of the applied stress. Here, $E_s$ represents the intrinsic material property of the material, by which the honeycomb cell walls (/connecting members) are made of. The notation $I$ represents the second moment of area of the cell walls, i.e. $I = bt^3/12$, where $t$ denotes the thickness of honeycomb cell wall. In the derivation of the expression of $E_{1U}$, the horizontal deflections away from point O are considered to be positive. In a similar way, the horizontal deflection of point B with respect to point O can be expressed as

$$\delta^h_{BO} = \left(\frac{P l_2^3 \sin\beta}{12 E_s I} - \frac{C l_1^3 \cos\beta}{12 E_s I}\right) \sin\beta \tag{7}$$

The distance of the point vertically below joint O and on the line AB (refer figure 5) is given by

$$\delta_O = \frac{l_2 \sin\beta l_1 \cos\alpha - l_1 \sin\alpha l_2 \cos\beta}{l_1 \cos\alpha - l_2 \cos\beta} \tag{8}$$

Considering a linear strain field along the line AB, the effective horizontal deformation of the RUCE is given by

$$\begin{aligned} \delta^h_1 &= \delta^h_{AO}\frac{\delta_O}{l_1 \sin\alpha} + \delta^h_{BO}\frac{\delta_O}{l_2 \sin\beta} \\ &= \frac{\sigma_1 L_y l_1^2 l_2^2 (l_1 + l_2)(\cos\alpha \sin\beta - \sin\alpha \cos\beta)^2}{E_s t^3 (l_1 \cos\alpha - l_2 \cos\beta)^2} \end{aligned} \tag{9}$$

The strain in direction-1 can be obtained from equation (9) as

$$\epsilon^h_1 = \frac{\sigma_1 L_y l_1^2 l_2^2 (l_1 + l_2)(\cos\alpha \sin\beta - \sin\alpha \cos\beta)^2}{E_s t^3 (l_1 \cos\alpha - l_2 \cos\beta)^3} \tag{10}$$

From equation (10), elastic modulus of a single RUCE in direction-1 is expressed as

$$E_{1U} = \frac{E_s t^3 (l_1 \cos\alpha - l_2 \cos\beta)^3}{L_y l_1^2 l_2^2 (l_1 + l_2)(\cos\alpha \sin\beta - \sin\alpha \cos\beta)^2} \tag{11}$$

It is important to note here that the above expression of $E_{1U}$ is for a non-idealized RUCE having

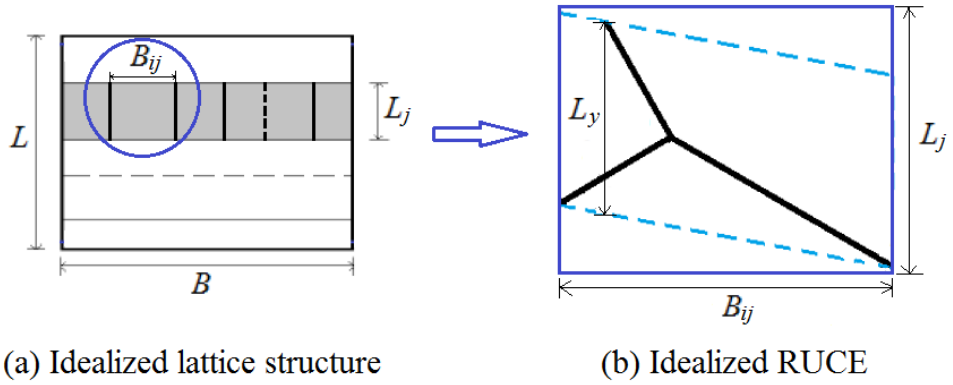


Figure 6: Idealization scheme of RUCE and the irregular lattice structure

a dimension of $L_y$ in direction-2. However, for assembling the local properties of RUCEs conveniently to the global level, it is essential to obtain the equivalent material property of an idealized RUCE ($E^I_{1U}$) that has a virtual dimension of $L_j$ (dimension of the $j^{th}$ strip in direction-2) as shown in figure 6. Considering a linear strain field, $E^I_{1U}$ can be obtained based on the deformation compatibility condition along direction-1, i.e. the deformation of the idealized RUCE and non-idealized RUCE in direction-1 should be equal

$$\frac{PB_{ij}}{A_{NI}E_{1U}} = \frac{PB_{ij}}{A_I E^I_{1U}} \tag{12}$$

Here $A_{NI} = L_y b$ and $A_I = L_j b$. The above equation can be reduced to

$$E^I_{1U} = E_{1U}\frac{L_y}{L_j} \tag{13}$$

*3.1.2. Longitudinal Young's modulus of the entire irregular lattice*

To obtain the longitudinal Young's modulus of the entire irregular lattice ($E_{1eq}$), a stress $\sigma_1$ is applied in direction-1 (refer figure 4). The deformation compatibility of $j^{th}$ strip ensures that the total deformation of the strip in direction-1 due to stress $\sigma_1$ ($\Delta_{1j}$) is the summation of individual deformations in direction-1 of each idealized RUCE ($\Delta_{1ij}$), while deformation of the idealized RUCEs of that strip in direction-2 are same. Thus for the $j^{th}$ strip

$$\Delta_{1j} = \sum_{i=1}^{m} \Delta_{1ij} \tag{14}$$

The equation (14) can be rewritten as

$$\epsilon_{1j} B_j = \sum_{i=1}^{m} \epsilon_{1ij} B_{ij} \tag{15}$$

where $\epsilon_{1j}$ and $B_j$ represent total strain and dimension in direction-1 for the $j^{th}$ strip (refer figure 6(a)). The notations used are described in subsection 2.1. Here $B_{ij} = (l_{1ij}\cos\alpha_{ij} - l_{2ij}\cos\beta_{ij})$ and $B_j =$

$\sum_{i=1}^{m} B_{ij}$. Equation (15) leads to

$$\frac{\sigma_1 B_j}{\hat{E_{1j}}} = \sum_{i=1}^{m} \frac{\sigma_1 B_{ij}}{E^I_{1Uij}} \tag{16}$$

From equation (16), equivalent Young's modulus of $j^{th}$ strip ($\hat{E_{1j}}$) can be expressed as

$$\hat{E_{1j}} = \frac{B_j}{\sum\limits_{i=1}^{m} \frac{B_{ij}}{E^I_{1Uij}}} \tag{17}$$

where $E^I_{1Uij}$ is the equivalent longitudinal elastic modulus in direction-1 of a single idealized RUCE positioned at ($i$,$j$) that can be obtained from equation (13).

In the next step, closed-form expression for equivalent longitudinal Young's modulus of the entire irregular lattice ($E_{1eq}$) is obtained using the equivalent longitudinal Young's modulus for a single strip ($\hat{E_{1j}}$). Employing the force equilibrium conditions and deformation compatibility condition we have

$$\sigma_1 L b = \sum_{j=1}^{n} \sigma_{1j} L_j b \tag{18}$$

where $L_j$ is the dimension of $j^{th}$ strip in direction-2 and $L = \sum\limits_{j=1}^{n} L_j$, as shown in figure 6(a). The notation $b$ represents the dimension of the lattice in the perpendicular direction to 1-2 plane. As strains in direction-1 for each of the $n$ strips are the same to satisfy the deformation compatibility condition, equation (18) leads to

$$E_{1eq} L = \sum_{j=1}^{n} \hat{E_{1j}} L_j \tag{19}$$

Using equation (17) and equation (19), the equivalent Young's modulus in direction-1 of the entire irregular honeycomb structure ($E_{1eq}$) can be expressed as

$$E_{1eq} = \frac{1}{L} \sum_{j=1}^{n} \frac{B_j L_j}{\sum\limits_{i=1}^{m} \frac{B_{ij}}{E^I_{1Uij}}} \tag{20}$$

From equations (11), (13) and (20), the expression for the longitudinal elastic modulus of the entire irregular lattice can be written as

$$E_{1eq} = \frac{E_s t^3}{L} \sum_{j=1}^{n} \frac{\sum\limits_{i=1}^{m} \left(l_{1ij} \cos\alpha_{ij} - l_{2ij} \cos\beta_{ij}\right)}{\sum\limits_{i=1}^{m} \frac{l^2_{1ij} l^2_{2ij} \left(l_{1ij} + l_{2ij}\right) \left(\cos\alpha_{ij} \sin\beta_{ij} - \sin\alpha_{ij} \cos\beta_{ij}\right)^2}{\left(l_{1ij} \cos\alpha_{ij} - l_{2ij} \cos\beta_{ij}\right)^2}} \tag{21}$$

*3.2. Transverse Young's modulus*

*3.2.1. Transverse Young's modulus for an idealized RUCE*

Stress $\sigma_2$ is applied in direction-2 to derive the expression of transverse Young's modulus for a RUCE ($E_{2U}$) as shown in figure 7. Total deformation of the RUCE in direction-2 consists of two components,

namely deformation of the cell wall OC in direction -2 and deformation of the cell walls OA and OB in direction-2. Deformation of the cell wall OC in direction -2 has two components: bending and rotation. Bending deformation of joint C with respect to O in direction-2 can be expressed as

$$\delta^{v}_{bCO} = \frac{W l_3^3 \cos^2\gamma}{12 E_s I} \tag{22}$$

where $W = \sigma_2 b\,(l_1 \cos\alpha - l_2 \cos\beta)$. The superscript $v$ is used to represent vertical direction of the

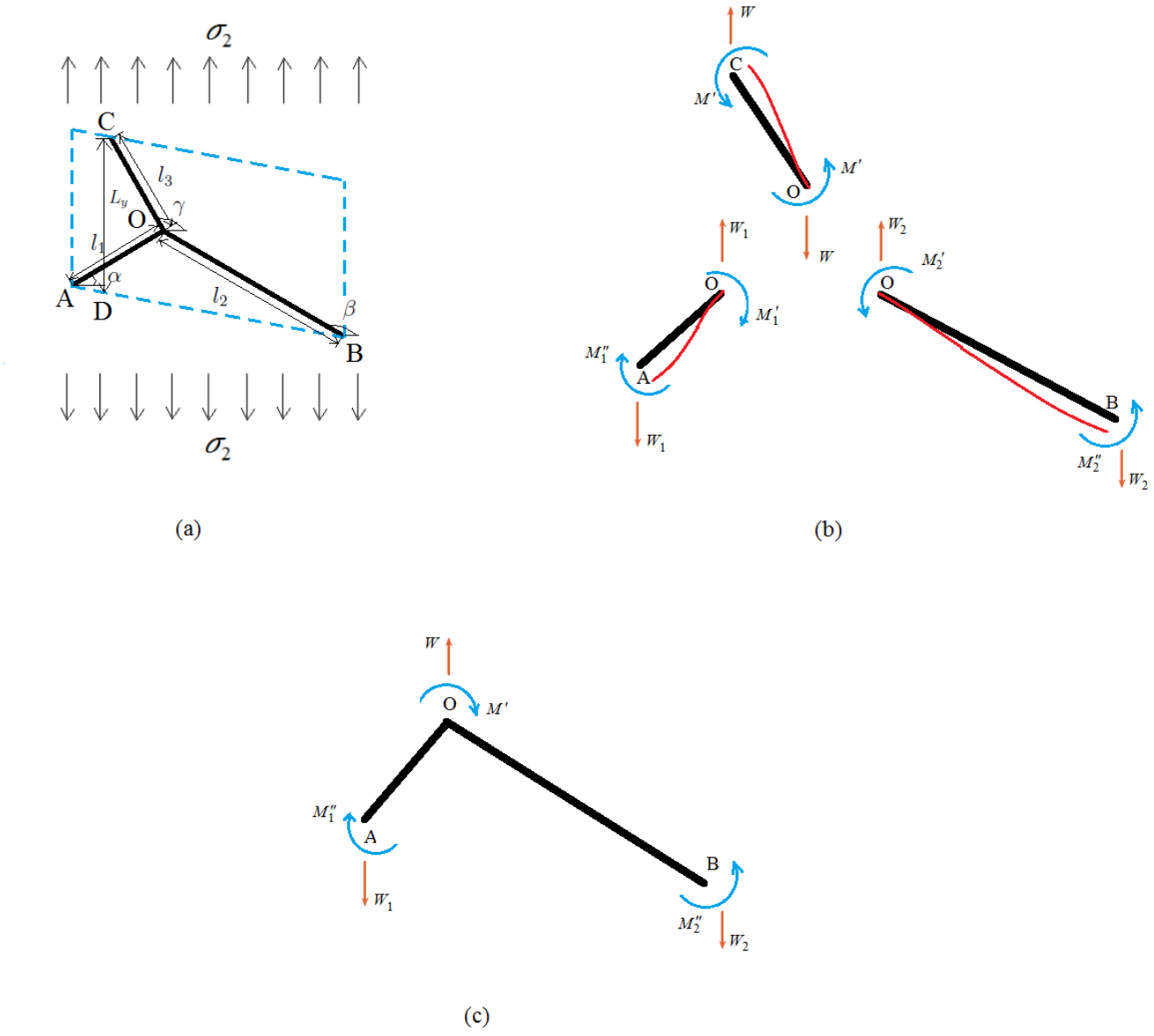


Figure 7: RUCE and free-body diagram for the proposed analysis of $E_{2U}$

applied stress. Expression of the bending moment acting at joint O of the free-body diagram of OC is $M' = -\dfrac{W l_3 \cos\gamma}{2}$. The bending moment $M'$ will be distributed to the members OA and OB according to their respective bending stiffness.Thus the components of $M'$ to members OA and OB

are: $M'_{OA} = \dfrac{l_2}{l_1+l_2}M'$ and $M'_{OB} = \dfrac{l_1}{l_1+l_2}M'$. Based on the standard formulae of Euler-Bernoulli beam theory (deflection at one end of a beam with length $l$ due to application of moment $M$ at the other end is given by: $\delta = \dfrac{Ml^2}{6EI}$), rotation of joint O can be expressed as $\phi = -\dfrac{M'_{OA}l_1}{6E_sI}$. Using the expressions of $M'_{OA}$ and $M'$, the vertical deformation of joint C with respect to joint O due to the rotation of joint O is given by

$$\delta^v_{rCO} = \frac{l_1 l_2 l_3^2 \cos^2\gamma}{12E_sI(l_1+l_2)}W \tag{23}$$

The expressions of the bending moments acting at joints O, A and B of the free-body diagrams of OA and OB are given by

$$M'_1 = \left(\frac{W_1 l_1 \cos\alpha}{2} + \frac{l_2}{l_1+l_2}M'\right) \tag{24}$$

$$M''_1 = \left(\frac{W_1 l_1 \cos\alpha}{2} - \frac{l_2}{l_1+l_2}M'\right) \tag{25}$$

$$M'_2 = \left(-\frac{W_2 l_2 \cos\beta}{2} - \frac{l_1}{l_1+l_2}M'\right) \tag{26}$$

$$\text{and} \quad M''_2 = \left(-\frac{W_2 l_2 \cos\beta}{2} + \frac{l_1}{l_1+l_2}M'\right) \tag{27}$$

Considering rotational equilibrium of the free-body diagram shown in figure 7(c), the expression of the vertical forces acting on joints A and B can be written as

$$W_1 = -\frac{l_2\cos\beta}{l_1\cos\alpha - l_2\cos\beta}W \tag{28}$$

$$\text{and} \quad W_2 = \frac{l_1\cos\alpha}{l_1\cos\alpha - l_2\cos\beta}W \tag{29}$$

Vertical deflections of the joints A and B in reference with joint O can be expressed as

$$\delta^v_{AO} = \frac{W_1 l_1^3\cos^2\alpha}{12E_sI} \tag{30}$$

$$\text{and} \quad \delta^v_{BO} = \frac{W_2 l_2^3\cos^2\beta}{12E_sI} \tag{31}$$

Considering a linear strain field, the deformation in direction-2 of the point vertically below point O and on the line joining A and B, with respect to joint O can be expressed as

$$\delta^v_O = \frac{\delta_{AO}(-l_2\cos\beta) + \delta_{BO}(l_1\cos\alpha)}{l_1\cos\alpha - l_2\cos\beta} \tag{32}$$

Replacing the expressions of $\delta^v_{AO}$ and $\delta^v_{BO}$, equation (32) can be written as

$$\delta^v_O = \frac{l_1^2 l_2^2\cos^2\alpha\cos^2\beta(l_1+l_2)}{12E_sI\left(l_1\cos\alpha - l_2\cos\beta\right)^2}W \tag{33}$$

The total deformation of a single RUCE in direction-2 can be expressed as

$$\begin{aligned}\delta_2^v &= \delta_{bCO}^v + \delta_{rCO}^v + \delta_O^v \\ &= \frac{W}{12E_sI}\left(l_3^2\cos^2\gamma\left(l_3+\frac{l_1l_2}{l_1+l_2}\right)+\frac{l_1^2l_2^2\left(l_1+l_2\right)\cos^2\alpha\cos^2\beta}{\left(l_1\cos\alpha-l_2\cos\beta\right)^2}\right)\end{aligned} \tag{34}$$

From equation (34), the strain in direction-2 can be obtained as

$$\epsilon_2^v = \frac{\sigma_2\left(l_1\cos\alpha-l_2\cos\beta\right)}{E_st^3L_y}\left(l_3^2\cos^2\gamma\left(l_3+\frac{l_1l_2}{l_1+l_2}\right)+\frac{l_1^2l_2^2\left(l_1+l_2\right)\cos^2\alpha\cos^2\beta}{\left(l_1\cos\alpha-l_2\cos\beta\right)^2}\right) \tag{35}$$

Using this, the transverse elastic modulus of the non-idealized RUCE can be given by

$$E_{2U} = \frac{E_st^3L_y}{\left(l_1\cos\alpha-l_2\cos\beta\right)}\left(l_3^2\cos^2\gamma\left(l_3+\frac{l_1l_2}{l_1+l_2}\right)+\frac{l_1^2l_2^2\left(l_1+l_2\right)\cos^2\alpha\cos^2\beta}{\left(l_1\cos\alpha-l_2\cos\beta\right)^2}\right)^{-1} \tag{36}$$

The above expression of $E_{2U}$ is for a non-idealized RUCE having a dimension of $L_y$ in direction-2. However, for assembling the local properties of RUCEs conveniently to the global level, it is essential to obtain the equivalent material property of an idealized RUCE ($E_{2U}^I$) that has a virtual dimension of $L_j$ (dimension of the $j^{th}$ strip in direction-2) as shown in figure 6. Considering a linear strain field, the $E_{2U}^I$ can be obtained based on the deformation compatibility condition along direction-2, i.e. deformation of the idealized RUCE and non-idealized RUCE in direction-2 should be equal. Enforcing this we have

$$\frac{WL_y}{AE_{2U}} = \frac{WL_j}{AE_{2U}^I} \tag{37}$$

where $A = B_{ij}b$. Thus the above equation reduces to

$$E_{2U}^I = E_{2U}\frac{L_j}{L_y} \tag{38}$$

*3.2.2. Transverse Young's modulus of the entire irregular lattice*

For deriving the expression of equivalent transverse Young's modulus for the entire irregular lattice ($E_{2eq}$), the transverse Young's modulus for the constituting idealized RUCEs ($E_{2U}^I$) are assembled as discussed in this section. Stress $\sigma_2$ is applied in direction-2 as depicted in figure 4. Considering the force equilibrium of the $j^{th}$ strip under stress $\sigma_2$,

$$\sigma_2 Bb = \left(\sum_{i=1}^{m}\sigma_{2ij}B_{ij}\right)b \tag{39}$$

According to deformation compatibility condition, strains of each idealized RUCE in direction-2 ($\epsilon_{2ij}$) of the $j^{th}$ strip are same. Equation (39) can be rewritten as

$$\hat{E_{2j}}\epsilon_{2j}B_j = \sum_{i=1}^{m}E_{2Uij}^I\epsilon_{2ij}B_{ij} \tag{40}$$

where $\epsilon_{2ij} = \epsilon_{2j}$, for $i = 1, 2...m$ in the $j^{th}$ strip. $\hat{E_{2j}}$ represents the equivalent elastic modulus in direction-2 of the $j^{th}$ strip. equation (40) leads to

$$\hat{E_{2j}} = \frac{\sum_{i=1}^{m} E^I_{2Uij} B_{ij}}{B_j} \tag{41}$$

Total deformation of the entire lattice in direction-2 ($\Delta_{2j}$) is the sum of individual deformations of each strip in that direction,

$$\epsilon^g_2 L = \sum_{j=1}^{n} \epsilon_{2j} L_j \tag{42}$$

where $\epsilon^g_2$ and $\epsilon_{2j}$ represent total strain of the entire lattice and strain of $j^{th}$ strip in direction-2, respectively. $L_j$ is the dimension of $j^{th}$ strip in direction-2 (refer figure 6(a)). Equation (42) can be rewritten as

$$\frac{\sigma_2 L}{E_{2eq}} = \sum_{j=1}^{n} \frac{\sigma_2 L_j}{\hat{E_{2j}}} \tag{43}$$

From equation (41) and equation (43), the transverse Young's modulus of the entire irregular lattice can be expressed as

$$E_{2eq} = \frac{L}{\sum_{j=1}^{n} \frac{L_j B_j}{\sum_{i=1}^{m} E^I_{2Uij} B_{ij}}} \tag{44}$$

From equation (36) and equation (38), the above expression can be re-written as

$$E_{2eq} = \frac{L E_s t^3}{\sum_{j=1}^{n} \frac{\sum_{i=1}^{m} \left(l_{1ij} \cos\alpha_{ij} - l_{2ij} \cos\beta_{ij}\right)}{\sum_{i=1}^{m} \left( l^2_{3ij} \cos^2\gamma_{ij} \left( l_{3ij} + \frac{l_{1ij} l_{2ij}}{l_{1ij} + l_{2ij}} \right) + \frac{l^2_{1ij} l^2_{2ij} (l_{1ij} + l_{2ij}) \cos^2\alpha_{ij} \cos^2\beta_{ij}}{(l_{1ij} \cos\alpha_{ij} - l_{2ij} \cos\beta_{ij})^2} \right)^{-1}}} \tag{45}$$

*3.3. Shear modulus*

*3.3.1. Shear modulus for an idealized RUCE*

To derive the expression of shear modulus ($G_{12U}$) for a single RUCE, shear stress $\tau$ is applied as shown in figure 8. Considering deformation compatibility and equilibrium conditions, it can be established that there is no relative movement of joint O with respect to joints A and B. From the deformation compatibility condition that the deflection of point O for the members OA and OB should be same in direction-2 ($\delta^s_{OA} = \delta^s_{OB}$) and the conditions of equilibrium for the free-body diagram of

AOB, the expressions of forces acting on points A and B can be written as

$$F_1 = \frac{\cot\alpha}{\cot\alpha - \cot\beta} F \tag{46}$$

$$F_2 = -\frac{\cot\beta}{\cot\alpha - \cot\beta} F \tag{47}$$

$$\text{and} \quad V_s = \frac{1}{\cot\alpha - \cot\beta} F \tag{48}$$

The horizontal movement of point O with respect to point A is given by

$$\delta^s_{OA} = \left( \frac{F_1 \sin\alpha l_1^3}{12 E_s I} - \frac{V_s \cos\alpha l_1^3}{12 E_s I} \right) \sin\alpha \tag{49}$$

Here the superscript $s$ is used to represent the applied shear stress. Replacing the expressions of $F_1$

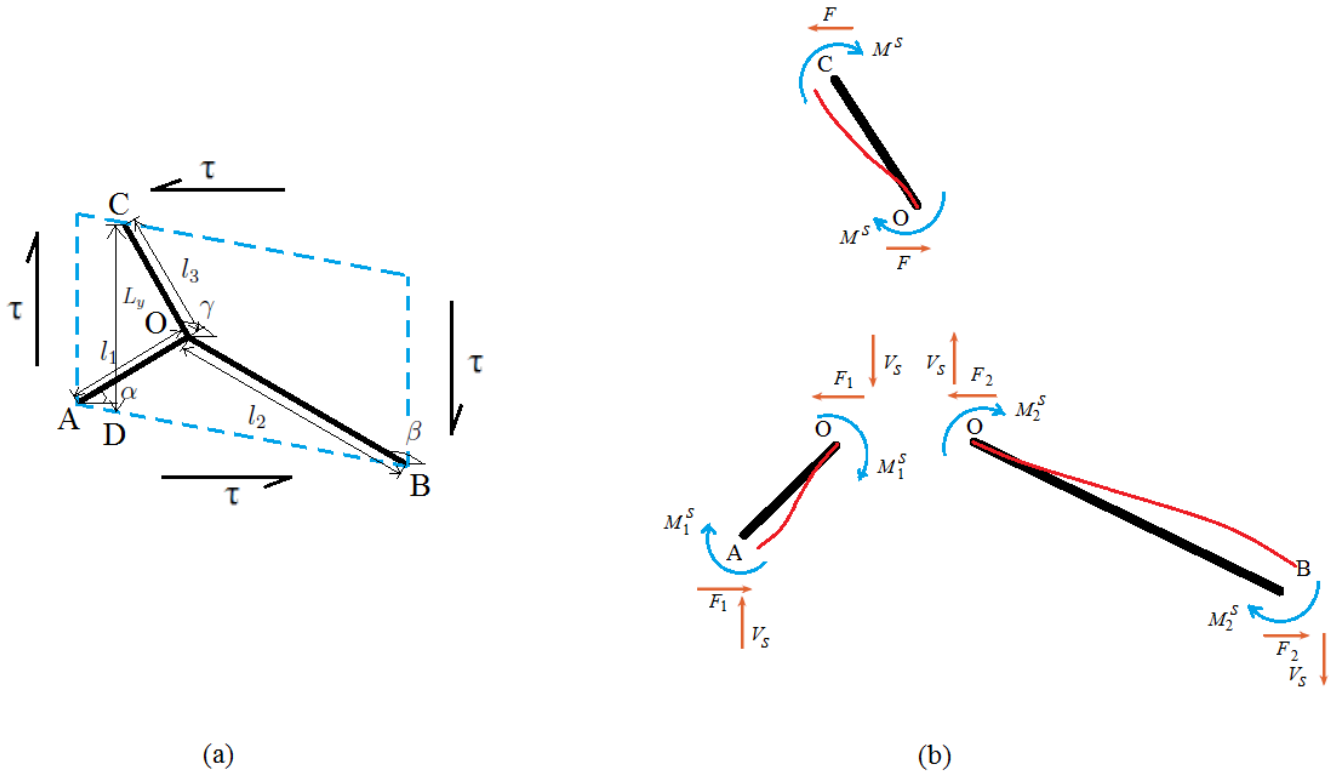


Figure 8: RUCE and free-body diagram for the proposed analysis of $G_{12U}$

and $V_s$ in the above expression, it can be obtained that $\delta^s_{OA} = \delta^s_{OB} = 0$. Thus, shear deformation of the entire unit cell is only contributed by the member OC. Deformation of point C in the direction of application of $\tau$ with respect to joint O consists of two components, bending deformation and rotational deformation. Bending deformation of point C in the direction of applied stress with respect to point O can be expressed as

$$\delta^s_{bCO} = \frac{F l_3^3 \sin^2\gamma}{12 E_s I} \tag{50}$$

where $F = \tau b\,(l_1 \cos\alpha - l_2 \cos\beta)$ and $M^s = \dfrac{F l_3 \sin\gamma}{2}$. The bending moment $M^s$ will be distributed to the members OA and OB according to their respective bending stiffness. Thus the components of $M^s$ to members OA and OB are: $M_1^s = \dfrac{l_2}{l_1+l_2} M^s$ and $M_2^s = \dfrac{l_1}{l_1+l_2} M^s$. Based on the standard formulae of the Euler-Bernoulli beam theory (deflection at one end of a beam with length $l$ due to application of moment $M$ at the other end is given by: $\delta = \dfrac{Ml^2}{6EI}$), rotation of joint O can be expressed as $\phi = \dfrac{l_1 l_2 M^s}{6E_s I(l_1+l_2)}$. Using these, the rotational deformation of point C in direction-1 with respect to point O can be expressed as

$$\delta_{rCO}^s = \phi l_3 \sin\gamma = \frac{l_1 l_2 l_3^2 \sin^2\gamma F}{12E_s I(l_1+l_2)} \tag{51}$$

Total deformation of point C in direction-1 with respect to point O is given by

$$\delta_{CO}^s = \delta_{bCO}^s + \delta_{rCO}^s = \frac{F l_3^2 \sin^2\gamma}{12E_s I}\left(l_3 + \frac{l_1 l_2}{l_1+l_2}\right) \tag{52}$$

From equation (52), replacing the expression of $F$, total shearing strain can be written as

$$\gamma_s = \frac{\tau\,(l_1\cos\alpha - l_2\cos\beta)\, l_3^2 \sin^2\gamma}{E_s t^3 L_y}\left(l_3 + \frac{l_1 l_2}{l_1+l_2}\right) \tag{53}$$

Thus, the expression for the shear modulus of a non-idealized RUCE is given by

$$G_{12U} = \frac{\tau}{\gamma_s} = \frac{E_s t^3 L_y}{l_3^2 \sin^2\gamma\,(l_1\cos\alpha - l_2\cos\beta)\left(l_3 + \frac{l_1 l_2}{l_1+l_2}\right)} \tag{54}$$

The above expression of $G_{12U}$ is for a non-idealized RUCE having a dimension of $L_y$ in direction-2. However, for assembling the local properties of RUCEs conveniently to the global level, it is essential to obtain the equivalent shear modulus of an idealized RUCE ($G_{12U}^I$) that has a virtual dimension of $L_j$ (dimension of the $j^{th}$ strip in direction-2) as shown in figure 6. Considering a linear strain field, the $G_{12U}^I$ can be obtained based on shear deformation compatibility condition i.e. shear deformation of the idealized RUCE and non-idealized RUCE should be equal.

$$\frac{\tau}{G_{12U}} L_y = \frac{\tau}{G_{12U}^I} L_j \tag{55}$$

From the above equation, expression for equivalent shear modulus of an idealized RUCE can be obtained as

$$G_{12U}^I = G_{12U}\frac{L_j}{L_y} \tag{56}$$

*3.3.2. Shear modulus of the entire irregular lattice*

Shear stress $\tau$ is applied as shown in figure 4 for obtaining shear modulus of the entire irregular lattice $G_{12eq}$. Considering the application of shear stress $\tau$ in the $j^{th}$ strip,

$$\tau B_j = \sum_{i=1}^{m} \tau_{ij} B_{ij} \tag{57}$$

Equation (57) can be rewritten as

$$\hat{G}_{12j} \gamma_j B_j = \sum_{i=1}^{m} G^I_{12Uij} \gamma_{ij} B_{ij} \tag{58}$$

where $\hat{G}_{12j}$ denotes the equivalent shear modulus of the $j^{th}$ strip. The notations $\gamma_j$ and $\gamma_{ij}$ represent the shear strains of $j^{th}$ strip and individual RUCEs of the $j^{th}$ strip, respectively. In equation (56), $G^I_{12Uij}$ is the shear modulus of an idealized RUCE positioned at $(i,j)$. From the deformation compatibility condition, $\gamma_j = \gamma_{ij}$ for $i = 1, 2, ..., m$ in the $j^{th}$ strip. Therefore, equation (58) leads to

$$\hat{G}_{12j} = \frac{\sum_{i=1}^{m} G^I_{12Uij} B_{ij}}{B_j} \tag{59}$$

Total shear deformation of the entire lattice structure under the application of shear stress $\tau$ is obtained by the summation of the individual shear deformations of $n$ number of strips. Thus

$$\gamma^g L = \sum_{j=1}^{n} \gamma_j L_j \tag{60}$$

where $\gamma^g$ denotes the shear strain of entire lattice. Using the definition of $G_{12}$, equation (60) can be written as

$$\frac{\tau}{G_{12eq}} L = \sum_{j=1}^{n} \frac{\tau_j}{\hat{G_{12j}}} L_j \tag{61}$$

where $\tau = \tau_j$. Using equation (59) and equation (61), equivalent shear modulus of the entire irregular lattice can be obtained as

$$G_{12eq} = \frac{L}{\sum_{j=1}^{n} \frac{L_j B_j}{\sum_{i=1}^{m} G^I_{12Uij} B_{ij}}} \tag{62}$$

Replacing the expression of $G^I_{12Uij}$ (refer equation (56)), the above equation leads to

$$G_{12eq} = \frac{L E_s t^3}{\sum_{j=1}^{n} \frac{\sum_{i=1}^{m} \left( l_{1ij} \cos\alpha_{ij} - l_{2ij} \cos\beta_{ij} \right)}{\sum_{i=1}^{m} \left( l^2_{3ij} \sin^2 \gamma_{ij} \left( l_{3ij} + \frac{l_{1ij} l_{2ij}}{l_{1ij} + l_{2ij}} \right) \right)^{-1}}} \tag{63}$$

*3.4. Poisson's ratio $\nu_{12}$*

*3.4.1. Poisson's ratio $\nu_{12}$ for an idealized RUCE*

Poisson's ratio of a single RUCE for the loading direction-1 ($\nu_{12U}$) is obtained as (refer figure 5)

$$\nu_{12U} = -\frac{\epsilon_2'}{\epsilon_1'} \tag{64}$$

where $\epsilon_1'$ and $\epsilon_2'$ are the strains of a non-idealized RUCE in direction-1 and direction-2 respectively due to loading in direction-1. $\epsilon_1'(=\epsilon_1^h)$ is obtained from equation (10). The vertical deflections of point A with respect to point O due to application of load in direction-1 (refer figure 5) are obtained as

$$\delta_{AO}' = -\left(\frac{Pl_1^3\sin\alpha}{12E_sI} - \frac{Cl_1^3\cos\alpha}{12E_sI}\right)\cos\alpha \tag{65}$$

where the first and second terms in the bracket represents the deflection of point A with respect to point O in the direction perpendicular to OA due to forces $P$ and $C$ respectively. In a similar way, the vertical deflection of point B with respect to point O can be expressed as

$$\delta_{BO}' = \left(\frac{Pl_2^3\sin\beta}{12E_sI} - \frac{Cl_1^3\cos\beta}{12E_sI}\right)\cos\beta \tag{66}$$

Similar to equation (32), deformation in direction-2 of the point vertically below point O and on the line joining A and B, with respect to joint O can be expressed as

$$\begin{aligned}\delta_O' &= \frac{\delta_{AO}'(-l_2\cos\beta) + \delta_{BO}'(l_1\cos\alpha)}{l_1\cos\alpha - l_2\cos\beta} \\ &= \frac{\sigma_1 l_1^2 l_2^2 L_y\,(l_1+l_2)\cos\alpha\cos\beta\,(\cos\alpha\sin\beta - \sin\alpha\cos\beta)}{E_s t^3\,(l_1\cos\alpha - l_2\cos\beta)^2}\end{aligned} \tag{67}$$

Thus the strain in direction-2 due to application of load in direction-1 can be obtained from equation (67) as

$$\epsilon_2' = \frac{\sigma_1 l_1^2 l_2^2\,(l_1+l_2)\cos\alpha\cos\beta\,(\cos\alpha\sin\beta - \sin\alpha\cos\beta)}{E_s t^3\,(l_1\cos\alpha - l_2\cos\beta)^2} \tag{68}$$

Using the definition of Poisson's ratio as shown in equation (64), the expression of Poisson's ratio corresponding to loading in direcion-1 for a non-idealized RUCE can be obtained as

$$\nu_{12U} = -\frac{\cos\alpha\cos\beta\,(l_1\cos\alpha - l_2\cos\beta)}{(\cos\alpha\sin\beta - \sin\alpha\cos\beta)\,L_y} \tag{69}$$

The above expression of $\nu_{12U}$ is for a non-idealized RUCE having a dimension of $L_y$ in direction-2. However, for assembling the local properties of RUCEs conveniently to the global level, it is essential to obtain the equivalent material property of an idealized RUCE ($\nu_{12U}^I$) that has a virtual dimension of $L_j$ (dimension of the $j^{th}$ strip in direction-2) in direction-2 as shown in figure 6. Considering a linear strain field, the $\nu_{12U}^I$ can be obtained based on deformation compatibility conditions: $\epsilon_1' B_{ij} = \epsilon_1'^I B_{ij}$ and $\epsilon_2' L_y = \epsilon_2'^I L_j$, where $(.)^I$ is used to indicate a parameter corresponding to idealized RUCE. Thus

the expression for Poisson's ratio of an idealized RUCE is given by

$$\nu_{12U}^{I} = \nu_{12U}\frac{L_y}{L_j} \tag{70}$$

*3.4.2. Poisson's ratio $\nu_{12}$ for the entire irregular lattice*

To derive the expression of equivalent Poisson's ratio of the entire irregular lattice for loading direction-1 ($\nu_{12eq}$), the Poisson's ratios for the constituting idealized RUCEs ($\nu_{12U}^{I}$) are assembled as discussed below. For obtaining $\nu_{12eq}$, stress $\sigma_1$ is applied as shown in figure 4. Considering the application of stress $\sigma_1$ in the $j^{th}$ strip, the following equation can be obtained from equation (15) using the basic definition of $\nu_{12}$,

$$-\frac{\epsilon_{2j}}{\hat{\nu}_{12j}}B_j = -\sum_{i=1}^{m}\frac{\epsilon_{2ij}B_{ij}}{\nu_{U12ij}^{I}} \tag{71}$$

where $\epsilon_{2j}$ and $\epsilon_{2ij}$ are the strains in direction-2 of $j^{th}$ strip and individual idealized RUCEs of $j^{th}$ strip respectively. $\nu_{U12ij}^{I}$ represents the Poisson's ratio for loading direction-1 of an idealized RUCE positioned at ($i$,$j$). $\hat{\nu}_{12j}$ denotes the equivalent Poisson's ratio of the $j^{th}$ strip for loading direction-1. To ensure the deformation compatibility condition $\epsilon_{2j} = \epsilon_{2ij}$ for $i = 1, 2, ..., m$ in the $j^{th}$ strip. Thus equation (71) reduces to

$$\hat{\nu}_{12j} = \frac{B_j}{\sum\limits_{i=1}^{m}\frac{B_{ij}}{\nu_{12Uij}^{I}}} \tag{72}$$

Total deformation of the entire lattice in direction-2 under the application of stress $\sigma_1$ is summation of the individual deformations of $n$ number of strips in direction-2

$$\epsilon_2^{g12}L = \sum_{j=1}^{n}\epsilon_{2j}L_j \tag{73}$$

where $\epsilon_2^{g12}$ is the total strain in direction-2. Using the basic definition of $\nu_{12}$ equation (73) can be rewritten as

$$\nu_{12eq}\epsilon_1^{g12}L = \sum_{j=1}^{n}\nu_{12j}\epsilon_{1j}L_j \tag{74}$$

where $\epsilon_1^{g12}$ and $\epsilon_{1j}$ denote the strain of entire lattice in direction-1 and strain of $j^{th}$ strip in direction-1 respectively. From the condition of deformation comparability the following condition can be established: $\epsilon_1^{g12} = \epsilon_{1j}$ for $j = 1, 2, ..., n$. Thus from equation (72) and 74,

$$\nu_{12eq} = \frac{1}{L}\sum_{j=1}^{n}\frac{BL_j}{\sum\limits_{i=1}^{m}\frac{B_{ij}}{\nu_{12Uij}^{I}}} \tag{75}$$

Replacing the expression of $\nu_{12Uij}^{I}$ from equation (69) and (70) in the above equation, the expression

of Poisson's ratio for loading direction-1 of the entire irregular lattice can be obtained as

$$\nu_{12eq} = -\frac{1}{L}\sum_{j=1}^{n}\frac{\sum_{i=1}^{m}\left(l_{1ij}\cos\alpha_{ij} - l_{2ij}\cos\beta_{ij}\right)}{\sum_{i=1}^{m}\frac{\left(\cos\alpha_{ij}\sin\beta_{ij} - \sin\alpha_{ij}\cos\beta_{ij}\right)}{\cos\alpha_{ij}\cos\beta_{ij}}} \tag{76}$$

*3.5. Poisson's ratio $\nu_{21}$*

*3.5.1. Poisson's ratio $\nu_{21}$ for an idealized RUCE*

Poisson's ratio of a single RUCE for the loading direction-2 ($\nu_{21U}$) is obtained as (refer figure 7)

$$\nu_{21U} = -\frac{\epsilon_1''}{\epsilon_2''} \tag{77}$$

where $\epsilon_1''$ and $\epsilon_2''$ are the strains of a non-idealized RUCE in direction-1 and direction-2 respectively due to loading in direction-2. $\epsilon_2''(=\epsilon_2^v)$ is obtained from equation (35). For deriving the expression of $\epsilon_1''$, the horizontal deflections of points A and B with respect to point O due to application of load in direction-2 are obtained as

$$\delta_{AO}'' = -\frac{W_1 l_1^3\cos\alpha\sin\alpha}{12E_sI} \tag{78}$$

$$\delta_{BO}'' = \frac{W_2 l_2^3\cos\beta\sin\beta}{12E_sI} \tag{79}$$

where $W_1$ and $W_2$ can be obtained from equation (28) and (29). Considering a linear strain field along the line AB, the effective deformation of the RUCE in direction-1 due to application of load in direction-2 is given by

$$\begin{aligned}\delta_1'' &= \delta_{AO}''\frac{\delta_O}{l_1\sin\alpha} + \delta_{BO}''\frac{\delta_O}{l_2\sin\beta}\\ &= \frac{W l_1^2 l_2^2\left(l_1+l_2\right)\cos\alpha\cos\beta\left(\cos\alpha\sin\beta - \sin\alpha\cos\beta\right)}{12E_sI\left(l_1\cos\alpha - l_2\cos\beta\right)^2}\end{aligned} \tag{80}$$

where $\delta_O$ is the distance of the point vertically below point O and on the line AB (refer equation (8)). From equation (80) the stain in direction-1 due to application of stress in direction-2 can be obtained as

$$\epsilon_1'' = \frac{\sigma_2 l_1^2 l_2^2\left(l_1+l_2\right)\cos\alpha\cos\beta\left(\cos\alpha\sin\beta - \sin\alpha\cos\beta\right)}{E_s t^3\left(l_1\cos\alpha - l_2\cos\beta\right)^2} \tag{81}$$

Using the definition of Poisson's ratio (refer equation (77)), the expression of Poisson's ratio corresponding to loading in direction-2 for a non-idealized RUCE can be obtained as

$$\nu_{21U} = -\frac{L_y l_1^2 l_2^2\left(l_1+l_2\right)\cos\alpha\cos\beta\left(\cos\alpha\sin\beta - \sin\alpha\cos\beta\right)}{\left(l_1\cos\alpha - l_2\cos\beta\right)^3\left(l_3^2\cos^2\gamma\left(l_3 + \frac{l_1 l_2}{l_1+l_2}\right) + \frac{l_1^2 l_2^2(l_1+l_2)\cos^2\alpha\cos^2\beta}{(l_1\cos\alpha - l_2\cos\beta)^2}\right)} \tag{82}$$

The above expression of $\nu_{21U}$ is for a non-idealized RUCE having a dimension of $L_y$ in direction-2. However, for assembling the local properties of RUCEs conveniently to the global level, it is essential

to obtain the equivalent material property of an idealized RUCE ($\nu^I_{21U}$) that has a virtual dimension of $L_j$ (dimension of the $j^{th}$ strip in direction-2) in direction-2 as shown in figure 6. Considering a linear strain field, the $\nu^I_{21U}$ can be obtained based on deformation compatibility conditions: $\epsilon''_1 B_{ij} = \epsilon''^I_1 B_{ij}$ and $\epsilon''_2 L_y = \epsilon''^I_2 L_j$, where $(.)^I$ is used to indicate a parameter corresponding to idealized RUCE. Thus the expression for Poisson's ratio of an idealized RUCE is given by

$$\nu^I_{21U} = \nu_{21U} \frac{L_j}{L_y} \tag{83}$$

*3.5.2. Poisson's ratio $\nu_{21}$ for the entire irregular lattice*

To derive the expression of equivalent Poisson's ratio for loading direction-2 of the entire irregular lattice structure ($\nu_{21eq}$), the Poisson's ratios for the constituting idealized RUCEs ($\nu^I_{21U}$) are assembled as discussed below. Stress $\sigma_2$ is applied in direction-2 for obtaining $\nu_{21eq}$, similar to the derivation of $E_{2eq}$ (as shown in figure 4). If the application of stress $\sigma_2$ in the $j^{th}$ strip is considered, total deformation of the $j^{th}$ strip in direction-1 is summation of individual deformations of the idealized RUCEs in direction-1 of that particular strip. Thus,

$$\epsilon_{1j} B_j = \sum_{i=1}^{m} \epsilon_{1ij} B_{ij} \tag{84}$$

Using the basic definition of $\nu_{21}$ equation (84) leads to

$$\hat{\nu}_{21j} \epsilon_{2j} B_j = \sum_{i=1}^{m} \nu^I_{21Uij} \epsilon_{2ij} B_{ij} \tag{85}$$

where $\hat{\nu}_{21j}$ denotes the equivalent Poisson's ratio for loading direction-2 of the $j^{th}$ strip. $\epsilon_{2j}$ and $\epsilon_{2ij}$ are the strains in direction-2 of $j^{th}$ strip and individual idealized RUCEs of $j^{th}$ strip, respectively. The quantity $\nu^I_{21Uij}$ represents the Poisson's ratio for loading direction-2 of an idealized RUCE located at ($i$,$j$). To ensure the deformation compatibility condition $\epsilon_{2j} = \epsilon_{2ij}$ for $i = 1, 2, ..., m$ in the $j^{th}$ strip. Thus equation (85) leads to

$$\hat{\nu_{21j}} = \frac{\sum_{i=1}^{m} \nu^I_{21Uij} B_{ij}}{B_j} \tag{86}$$

Total deformation of the entire lattice in direction-2 due to application of stress $\sigma_2$ is summation of the individual deformations in direction-2 of $n$ number of strips. Thus

$$\epsilon^{g21}_2 L = \sum_{j=1}^{n} \epsilon_{2j} L_j \tag{87}$$

where $\epsilon^{g21}_2$ is the strain of the entire lattice in direction-2. By definition of $\nu_{21}$ equation (87) leads to

$$\frac{\epsilon^{g21}_1}{\nu_{21eq}} L = \sum_{j=1}^{n} \frac{\epsilon_{1j}}{\hat{\nu_{21j}}} L_j \tag{88}$$

where $\epsilon_1^{g21}$ is the strain of the entire lattice in direction-1. From the condition of deformation comparability the following equality is established: $\epsilon_1^{g21} = \epsilon_{1j}$ for $j = 1, 2, ..., n$. Using equation (86) and (88), the equivalent Poisson's ratio for loading direction-2 of the entire irregular lattice structure can be obtained as

$$\nu_{21eq} = \frac{L}{\sum_{j=1}^{n} \frac{B_j}{\sum_{i=1}^{m} \frac{\nu_{21Uij}^I B_{ij}}{L_y}}} \tag{89}$$

Replacing the expression of $\nu_{21Uij}^I$ from equation (83), the above equation can be rewritten as

$$\nu_{21eq} = -\frac{L}{\sum_{j=1}^{n} \frac{\sum_{i=1}^{m} \left(l_{1ij}\cos\alpha_{ij} - l_{2ij}\cos\beta_{ij}\right)}{\sum_{i=1}^{m} \frac{l_{1ij}^2 l_{2ij}^2 \left(l_{1ij}+l_{2ij}\right)\cos\alpha_{ij}\cos\beta_{ij}\left(\cos\alpha_{ij}\sin\beta_{ij} - \sin\alpha_{ij}\cos\beta_{ij}\right)}{\left(l_{1ij}\cos\alpha_{ij} - l_{2ij}\cos\beta_{ij}\right)^2 \left(l_{3ij}^2\cos^2\gamma_{ij}\left(l_{3ij} + \frac{l_{1ij}l_{2ij}}{l_{1ij}+l_{2ij}}\right) + \frac{l_{1ij}^2 l_{2ij}^2 (l_{1ij}+l_{2ij})\cos^2\alpha_{ij}\cos^2\beta_{ij}}{\left(l_{1ij}\cos\alpha_{ij} - l_{2ij}\cos\beta_{ij}\right)^2}\right)}}} \tag{90}$$

The negative sign in the expression of Poisson's ratios (refer equation (76) and equation (90)) does not indicate any auxetic characteristics in the present context; rather it is due to the fact that $\beta_{ij} > 90°$ as shown in figure 7.

### *3.6. Remark 1: regular lattices*

The closed-form expressions of all the in-plane elastic moduli for irregular lattices in subsection 3.1 - 3.5 can be reduced to the formulae provided by Gibson and Ashby (1999) in the special case of uniform honeycombs as described in Table 1 (subscript $GA$ is used as denotation for the formulae of regular honeycomb). With reference to the notations used for a regular honeycomb by Gibson and Ashby (1999) as shown in figure 3(d), the notations of the present paper for regular honeycombs can be expressed as: $L = n(h + l\sin\theta)$; $l_{1ij} = l_{2ij} = l_{3ij} = l$; $\alpha_{ij} = \theta$; $\beta_{ij} = 180° - \theta$; $\gamma_{ij} = 90°$, for all $i$ and $j$. Using these transformations in equation (21), (45), (63), (76) and (90), the expressions of longitudinal and transverse elastic moduli, shear modulus and Poisson's ratios for regular honeycomb can be obtained, respectively.

In the case of regular uniform honeycombs with $\theta = 30°$, we have

$$\frac{E_1^*}{E_s} = \frac{E_2^*}{E_s} = 2.3\left(\frac{t}{l}\right)^3 \tag{91}$$

where $E_1^*$ and $E_2^*$ denote the Young moduli of uniform regular honeycombs in longitudinal and transverse direction respectively. Similarly, in the case of shear modulus for regular uniform honeycombs

Table 1: Summary of formulae for effective in-plane elastic properties of hexagonal lattices

| Parameter | Structural configuration | In-plane elastic properties | | | | |
|---|---|---|---|---|---|---|
| | | $E_1$ | $E_2$ | $G_{12}$ | $\nu_{12}$ | $\nu_{21}$ |
| Regular lattice |  Figure: Regular lattice   Figure: Unit Cell | $E_{1GA} = E_s\left(\frac{t}{l}\right)^3 \frac{\cos\theta}{(\frac{h}{l}+\sin\theta)\sin^2\theta}$ | $E_{2GA} = E_s\left(\frac{t}{l}\right)^3 \frac{(\frac{h}{l}+\sin\theta)}{\cos^3\theta}$ | $G_{12GA} = E_s\left(\frac{t}{l}\right)^3 \frac{\left(\frac{h}{l}+\sin\theta\right)}{\left(\frac{h}{l}\right)^2(1+2\frac{h}{l})\cos\theta}$ | $\nu_{12GA} = \frac{\cos^2\theta}{(\frac{h}{l}+\sin\theta)\sin\theta}$ | $\nu_{21GA} = \frac{(\frac{h}{l}+\sin\theta)\sin\theta}{\cos^2\theta}$ |
| Irregular lattice |  Figure: Irregular lattice   Figure: RUCE | $E_{1eq} = \frac{E_s t^3}{L}\sum_{j=1}^{n}\frac{\sum_{i=1}^{m}(l_{1ij}\cos\alpha_{ij} - l_{2ij}\cos\beta_{ij})}{\sum_{i=1}^{m}\frac{l_{1ij}^2 l_{2ij}^2(l_{1ij}+l_{2ij})(\cos\alpha_{ij}\sin\beta_{ij}-\sin\alpha_{ij}\cos\beta_{ij})^2}{(l_{1ij}\cos\alpha_{ij}-l_{2ij}\cos\beta_{ij})^2}}$ | $E_{2eq} = \frac{LE_s t^3}{\sum_{i=1}^{m}(l_{1ij}\cos\alpha_{ij} - l_{2ij}\cos\beta_{ij})\sum_{j=1}^{n}\frac{\sum_{i=1}^{m}\left(l_{3ij}^2\cos^2\gamma_{ij}\left(l_{3ij}+\frac{l_{1ij}l_{2ij}}{l_{1ij}+l_{2ij}}\right)+\frac{l_{1ij}^2 l_{2ij}^2(l_{1ij}+l_{2ij})\cos^2\alpha_{ij}\cos^2\beta_{ij}}{(l_{1ij}\cos\alpha_{ij}-l_{2ij}\cos\beta_{ij})^2}\right)^{-1}}{\sum_{i=1}^{m}\left(l_{3ij}^2\cos^2\gamma_{ij}\left(l_{3ij}+\frac{l_{1ij}l_{2ij}}{l_{1ij}+l_{2ij}}\right)\right)^{-1}}}$ | $G_{12eq} = \frac{LE_s t^3}{\sum_{i=1}^{m}(l_{1ij}\cos\alpha_{ij} - l_{2ij}\cos\beta_{ij})\sum_{j=1}^{n}\frac{\sum_{i=1}^{m}\left(l_{3ij}^2\sin^2\gamma_{ij}\left(l_{3ij}+\frac{l_{1ij}l_{2ij}}{l_{1ij}+l_{2ij}}\right)\right)^{-1}}{\sum_{i=1}^{m}\left(l_{3ij}^2\sin^2\gamma_{ij}\left(l_{3ij}+\frac{l_{1ij}l_{2ij}}{l_{1ij}+l_{2ij}}\right)\right)^{-1}}}$ | $\nu_{12eq} = -\frac{1}{L}\sum_{j=1}^{n}\frac{\sum_{i=1}^{m}(l_{1ij}\cos\alpha_{ij} - l_{2ij}\cos\beta_{ij})}{\sum_{i=1}^{m}\frac{(\cos\alpha_{ij}\sin\beta_{ij}-\sin\alpha_{ij}\cos\beta_{ij})}{\cos\alpha_{ij}\cos\beta_{ij}}}$ | $\nu_{21eq} = -\frac{L}{\sum_{i=1}^{m}(l_{1ij}\cos\alpha_{ij} - l_{2ij}\cos\beta_{ij})\sum_{j=1}^{n}\frac{l_{1ij}^2 l_{2ij}^2(l_{1ij}+l_{2ij})\cos\alpha_{ij}\cos\beta_{ij}(\cos\alpha_{ij}\sin\beta_{ij}-\sin\alpha_{ij}\cos\beta_{ij})}{\sum_{i=1}^{m}(l_{1ij}\cos\alpha_{ij}-l_{2ij}\cos\beta_{ij})^2\left(l_{3ij}^2\cos^2\gamma_{ij}\left(l_{3ij}+\frac{l_{1ij}l_{2ij}}{l_{1ij}+l_{2ij}}\right)+\frac{l_{1ij}^2 l_{2ij}^2(l_{1ij}+l_{2ij})\cos^2\alpha_{ij}\cos^2\beta_{ij}}{(l_{1ij}\cos\alpha_{ij}-l_{2ij}\cos\beta_{ij})^2}\right)}}$ |

($\theta = 30^\circ$)

$$\frac{G_{12}^*}{E_s} = 0.57 \left(\frac{t}{l}\right)^3 \tag{92}$$

where $G_{12}^*$ represents the shear modulus of uniform regular honeycombs. Regular honeycombs satisfy the reciprocal theorem: $E_2^*\nu_{12}^* = E_1^*\nu_{21}^*$, where $\nu_{12}^*$ and $\nu_{21}^*$ denote the Poisson's ratios of regular honeycombs. It is noteworthy that for regular uniform honeycombs, the Poisson's ratios become unity (i.e. $\nu_{12}^* = \nu_{21}^* = 1$) and the regular uniform honeycombs correctly obey the relation $G = E/2(1+\nu)$, where $E$, $G$ and $\nu$ represent Young's modulus, shear modulus and Poisson's ratio of isotropic solids respectively. These relationships in general do not hold for irregular honeycombs considered in this work.

### *3.7. Remark 2: effects of spatially random variation of intrinsic material property*

From the preceding sections it is observed that the in-plane Poisson's ratios do not depend on the intrinsic material properties of the lattice. Thus the effect of spatially random variation of intrinsic material properties (and the compound effects for spatial variation of both intrinsic material property and structural geometry) on the two Young's moduli and shear modulus are investigated as a part of this article.

#### *3.7.1. Compound effects on the in-plane elastic moduli for spatial variation of both intrinsic material property and structural geometry*

Closed-form formulae are derived in this section to account for the compound effect on the in-plane elastic moduli due to spatial variation of both material property and structural geometry. From equation (10), elastic modulus of a single RUCE (located at $i^{th}$ column and $j^{th}$ row of the lattice) in direction-1 with randomly varying properties can be expressed as

$$E_{1Uij} = \frac{E_{sij} t^3 \left(l_{1ij}\cos\alpha_{ij} - l_{2ij}\cos\beta_{ij}\right)^3}{L_y l_{1ij}^2 l_{2ij}^2 \left(l_{1ij} + l_{2ij}\right)\left(\cos\alpha_{ij}\sin\beta_{ij} - \sin\alpha_{ij}\cos\beta_{ij}\right)^2} \tag{93}$$

Here $E_{sij}$ is the intrinsic material property of a RUCE located at $i^{th}$ column and $j^{th}$ row of the lattice. Noting the relationship in equation (13) and using the expression in equation (20), the effective longitudinal Young's modulus for compound spatial variation of intrinsic material properties and structural geometry as

$$E_{1eq} = \frac{t^3}{L} \sum_{j=1}^{n} \frac{\sum_{i=1}^{m} \left(l_{1ij}\cos\alpha_{ij} - l_{2ij}\cos\beta_{ij}\right)}{\sum_{i=1}^{m} \frac{l_{1ij}^2 l_{2ij}^2 \left(l_{1ij} + l_{2ij}\right)\left(\cos\alpha_{ij}\sin\beta_{ij} - \sin\alpha_{ij}\cos\beta_{ij}\right)^2}{E_{sij}\left(\left(l_{1ij}\cos\alpha_{ij} - l_{2ij}\cos\beta_{ij}\right)^2\right)}} \tag{94}$$

This expression enables the consideration of simultaneous spatial variation of intrinsic material property and spatially random structural geometry.

From equations (36), (38) and (44), the effective transverse Young's modulus for compound spatial variation of intrinsic material properties and structural geometry can be obtained as:

$$E_{2eq} = \frac{Lt^3}{\sum_{i=1}^{m}\left(l_{1ij}\cos\alpha_{ij} - l_{2ij}\cos\beta_{ij}\right)} \Bigg/ \sum_{j=1}^{n} \frac{\sum_{i=1}^{m}\left(l_{1ij}\cos\alpha_{ij} - l_{2ij}\cos\beta_{ij}\right)}{\sum_{i=1}^{m} E_{sij}\left(l_{3ij}^2\cos^2\gamma_{ij}\left(l_{3ij} + \frac{l_{1ij}l_{2ij}}{l_{1ij}+l_{2ij}}\right) + \frac{l_{1ij}^2 l_{2ij}^2 (l_{1ij}+l_{2ij})\cos^2\alpha_{ij}\cos^2\beta_{ij}}{(l_{1ij}\cos\alpha_{ij} - l_{2ij}\cos\beta_{ij})^2}\right)^{-1}} \tag{95}$$

From equations equation (54), (56) and (62), the effective shear modulus for compound spatial variation of intrinsic material properties and structural geometry can be obtained as:

$$G_{12eq} = \frac{Lt^3}{\sum_{i=1}^{m}\left(l_{1ij}\cos\alpha_{ij} - l_{2ij}\cos\beta_{ij}\right)} \Bigg/ \sum_{j=1}^{n} \frac{\sum_{i=1}^{m}\left(l_{1ij}\cos\alpha_{ij} - l_{2ij}\cos\beta_{ij}\right)}{\sum_{i=1}^{m} E_{sij}\left(l_{3ij}^2\sin^2\gamma_{ij}\left(l_{3ij} + \frac{l_{1ij}l_{2ij}}{l_{1ij}+l_{2ij}}\right)\right)^{-1}} \tag{96}$$

The above expressions can account for the effect of both spatially random variation of structural and material property enabling us to quantify the compound effect arising due to the simultaneous variation of both quantities on the in-plane elastic moduli. The in-plane Poisson's ratios do not depend on the intrinsic material properties of the lattice. Thus we have investigated the compound effects for spatial variation of both intrinsic material property and structural geometry in case of the Young's moduli and shear modulus. The expressions of Poisson's ratios for the case of compound variation will remain same as provided in equations (76) and (90).

*3.7.2. Effect on the in-plane elastic moduli for spatially random variation of intrinsic material properties only*

With reference to the notations used for a regular honeycomb by Gibson and Ashby (1999) (as shown in figure 3(d)), the notations of the present paper for regular honeycombs can be expressed as: $L = n(h + l\sin\theta)$; $l_{1ij} = l_{2ij} = l_{3ij} = l$; $\alpha_{ij} = \theta$; $\beta_{ij} = 180^\circ - \theta$; $\gamma_{ij} = 90^\circ$, for all $i$ and $j$. Using these transformations in case of the variation of only material properties, the closed-form formulae for compound variation of material and geometric properties (equations 94–96) can be reduced to:

$$E_{1eq} = \kappa_1 \left(\frac{t}{l}\right)^3 \frac{\cos\theta}{(\frac{h}{l} + \sin\theta)\sin^2\theta} \tag{97}$$

$$E_{2eq} = \kappa_2 \left(\frac{t}{l}\right)^3 \frac{(\frac{h}{l} + \sin\theta)}{\cos^3\theta} \tag{98}$$

$$\text{and} \quad G_{12eq} = \kappa_2 \left(\frac{t}{l}\right)^3 \frac{\left(\frac{h}{l} + \sin\theta\right)}{\left(\frac{h}{l}\right)^2 (1 + 2\frac{h}{l})\cos\theta} \tag{99}$$

Resemblance of the above equations with the expressions provided by Gibson and Ashby (1999) is noteworthy; the generalization in terms of spatially varying material properties are clearly accounted by the two multiplication factors $\kappa_1$ and $\kappa_2$. These two factors arising due to the consideration of spatially random variation of intrinsic material properties can be expressed as

$$\kappa_1 = \frac{m}{n} \sum_{j=1}^{n} \frac{1}{\sum_{i=1}^{m} \frac{1}{E_{sij}}} \tag{100}$$

$$\text{and} \quad \kappa_2 = \frac{n}{m} \frac{1}{\sum_{j=1}^{n} \frac{1}{\sum_{i=1}^{m} E_{sij}}} \tag{101}$$

The in-plane Poisson's ratios do not depend on the intrinsic material properties of the lattice. Thus we have investigated the individual effect for spatial variation of intrinsic material property in case of the Young's moduli and shear modulus. The expressions of Poisson's ratios for the case of intrinsic material property variation will remain same as the formulae provided by Gibson and Ashby (1999) (i.e. $\nu_{12eq} = \nu_{12GA}$ and $\nu_{21eq} = \nu_{21GA}$; refer to Table 1). In the special case when there is no spatial variabilities in the intrinsic material properties of the lattice, all $E_{s_{ij}}$ becomes identical (i.e. $E_{sij} = E_s$, for $i = 1, 2, 3, ..., m$ and $j = 1, 2, 3, ..., n$) and subsequently $\kappa_1$ and $\kappa_2$ become exactly $E_s$. This confirms that the expressions in equation (100) and equation (101) give the necessary generalisations of the classical expressions of Gibson and Ashby (1999) through equation (97), equation (98) and equation (99).

## 4. Results and discussion

A finite element code is developed to obtain the in-plane elastic moduli numerically for lattices with general spatial random structural variations. The developed finite element code is capable of accepting the number of cells in two perpendicular directions and spatially irregular structural forms/ intrinsic material property distribution as input to obtain the corresponding five in-plane elastic moduli as output. The main purpose of the finite element model in context of the present study is to validate the proposed analytical formulae (refer to section 3) for equivalent in-plane elastic moduli of irregular lattices. Each connecting member has been modelled as standard Euler-Bernoulli beam element neglecting axial and shear deformation with the assumption of high axial rigidity and low cell wall thickness respectively. The finite element code is validated with the results from scientific literature corresponding to regular configuration (Gibson and Ashby, 1999). The results for validation of five in-plane elastic moduli are furnished in figure 9 along with convergence study for a regular lattice

with cell angle 30° and $h/l = 1$ (symbols are in accordance with the unit cell adopted by Gibson and Ashby (1999); refer to figure 3(d)). The convergence study is carried out for the five in-plane elastic moduli with number of RUCEs to ensure that the equivalent global behaviour of the entire lattice is accounted by avoiding any localised deformation due to boundary effect. The finite element code obtains the ratio reasonably close to 1 for 529 RUCEs or less. As considering a far smaller number of RUCEs for the analysis may be insufficient to account for the effect of structural randomness in global behaviour of the entire lattice, a relatively larger size of lattice (having a total of 961 RUCEs) is adopted for all the subsequent analyses to capture the effect of spatially random structural irregularity comprehensively.

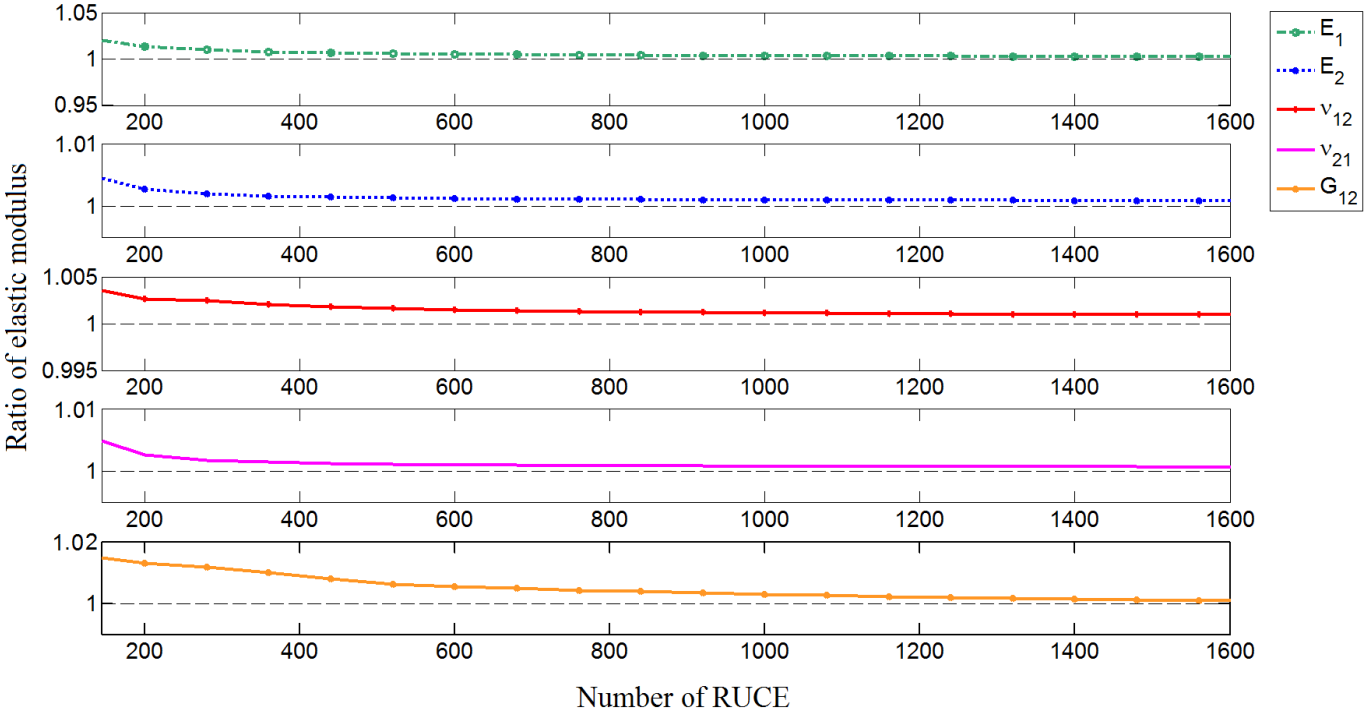


Figure 9: Convergence study and validation of finite element model for obtaining elastic moduli of regular hexagonal lattices. The results are shown as a ratio for a particular elastic modulus obtained using the finite element code and from the formula provided by Gibson and Ashby (1999)

The analytical formulae developed in section 3 are capable of obtaining the equivalent in-plane properties for irregular hexagonal lattices from known spatial configuration of structural geometry and material properties. Characterization of such irregularities in material micro-structure with hexagonal configuration can be performed by common techniques like digital image analysis. To quantify the variation in elastic moduli of hexagonal lattices due to spatial irregularity, structural geometry and material properties can be perturbed as described in subsection 2.2 following a random distribution. From the closed-form expressions of equivalent in-plane elastic moduli derived in section 3, it is evident

that all the in-plane elastic moduli depend on $l_1$, $l_2$, $l_3$, $\alpha$, $\beta$, $\gamma$ and $t$ (refer Table 1) of all the constituent RUCEs. The dimension of the entire lattice in direction-2 ($L$) is an inherent function of the structural geometries mentioned above. Two Young's moduli and the shear modulus are also dependent on the intrinsic material property $E_s$ in addition to the geometric attributes. The formulae derived in this paper are valid for small strain allowing the non-linearity caused by beam-column effect to be neglected. Only bending deformation is considered as the effect due to axial and shear deformation are negligible because of high axial rigidity and small bending thickness compared to the other dimensions of a RUCE, respectively.

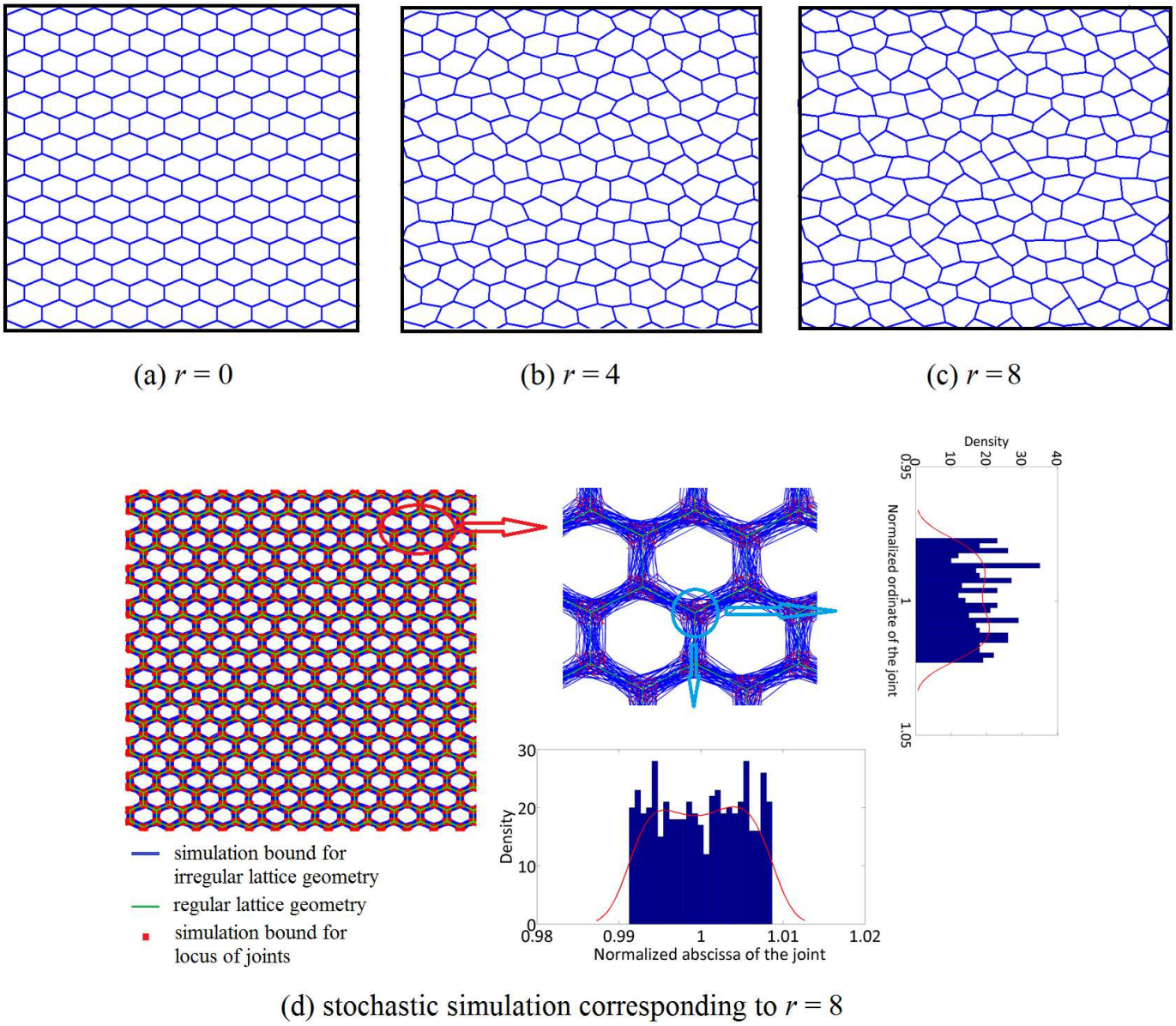


Figure 10: (a-c) Representative configuration of spatially random irregular hexagonal lattices corresponding to different degree of irregularity for a single random realization (d) Simulation bound for the contour of irregular lattice configurations considering multiple random realizations and statistical interpretation

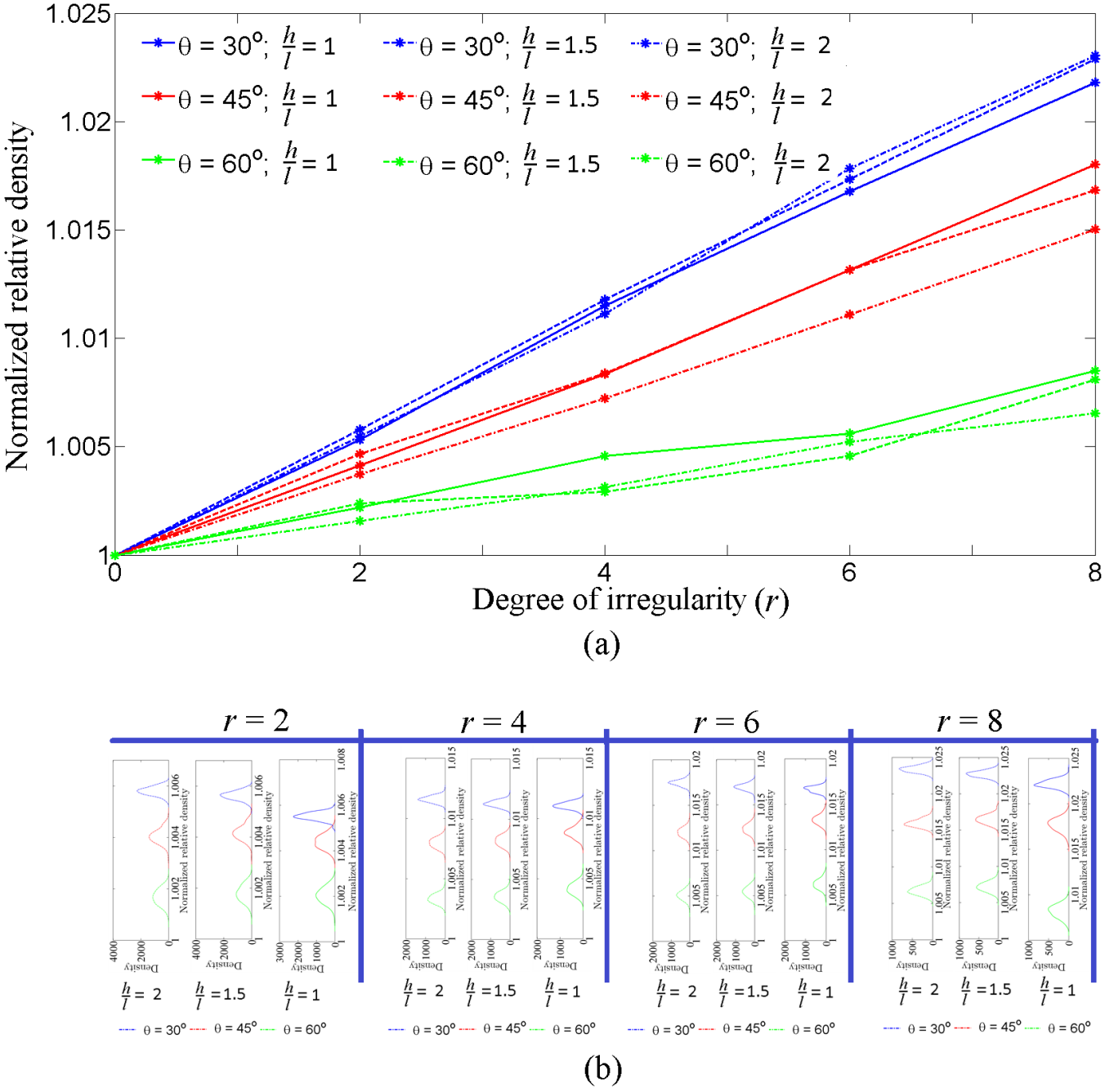


Figure 11: (a) Effect of irregularity on mean normalized relative density of hexagonal lattices (b) Probabilistic characterization for relative densities corresponding to different degree of irregularity ($r$)

Here only spatially random structural variation is discussed (the case of random intrinsic material property variation (including the compound effects) is discussed in subsection 3.7). Results have been obtained following a probabilistic framework involving 10,000 random realizations. In each realization, the nodes corresponding to deterministic configuration are allowed to move randomly (following a uniform random distribution) within a circular bound for obtaining the spatially random structural configuration as discussed in subsection 2.2. Thus each realization possess spatially random values of

the structural attributes ( $l_1$, $l_2$, $l_3$, $\alpha$, $\beta$ and $\gamma$) corresponding to each RUCE. Figure 10(a-c) show representative structural configurations of spatially random irregular hexagonal lattices corresponding to three different degree of irregularities ($r$) considering a single random realization of the Monte Carlo simulation. Figure 10(d) presents simulation bound for the contour of irregular lattice configurations considering multiple random realizations indicating the contour of nodes and the connecting members. Statistical distributions of normalized movement in terms of abscissa and ordinate (normalized with respect to the corresponding value of deterministic abscissa and ordinate for the considered node) for a particular node are shown in the zoomed in view. The distributions clearly indicate a uniform random distribution, which is followed in this study. However, to understand the physical interpretation of the disorder in terms of degree of irregularity ($r$), let us consider a regular uniform hexagonal lattice with $h = l$ and $\theta = 30°$. From the equation (2), it can be obtained that, $r_d = 0.257l$, for $r = 8$ (refer to figure 3(d) for the dimensions $h$ and $l$). Thus, it can be understood that simultaneously random movement of all the nodes of lattice within a circular bound of radius $r_d = 0.257l$ results in a significant disorder in the lattice structure. This is also evident from the figure 10(c).

Results are presented for three different $h/l$ ratios (1, 1.5 and 2) with a small $t/l$ value ($\sim 10^{-2}$) corresponding to respective deterministic lattice configurations (refer figure 3(d)) to quantify the variability in the in-plane elastic moduli due to structural irregularity. For each of the $h/l$ ratios, three different cell angles ($\theta$) are considered corresponding to deterministic configuration (30°, 45° and 60°). As the two Young's moduli and the shear modulus for low density lattices are proportional to $E_s\rho^3$ (Zhu et al., 2001), the non-dimensional results for in-plane elastic moduli $E_1$, $E_2$, $\nu_{12}$, $\nu_{21}$ and $G_{12}$ are presented as: $\bar{E_1} = \dfrac{E_{1eq}}{E_s\rho^3}$ , $\bar{E_2} = \dfrac{E_{2eq}}{E_s\rho^3}$ , $\bar{\nu_{12}} = \nu_{12eq}$ , $\bar{\nu_{21}} = \nu_{21eq}$ and $\bar{G_{12}} = \dfrac{G_{12eq}}{E_s\rho^3}$ respectively, where ' $(\bar{.})$ ' denotes the non-dimensional elastic modulus and $\rho$ is the relative density of the lattice (defined as a ratio of the planar area of solid to the total planar area of the lattice).

Figure 11 presents the effect of irregularity on relative density of hexagonal lattices along with their probabilistic characteristics for different structural configurations. Non-dimensional results for relative density have been obtained as a ratio of the relative density for a particular irregular structural configuration and relative density for the corresponding regular (/deterministic) configuration. The figure shows that normalized relative density increases with the increase of irregularity for all the deterministic structural configurations. It is interesting to notice that even though the regular uniform deterministic hexagonal configuration ($\theta = 30°; h/l = 1$) is the most efficient space filling pattern, it is also the most sensitive configuration to irregularity for relative density. The effect of spatially random structural irregularity decreases with the increase of deterministic cell angle ($\theta$) in terms of the mean

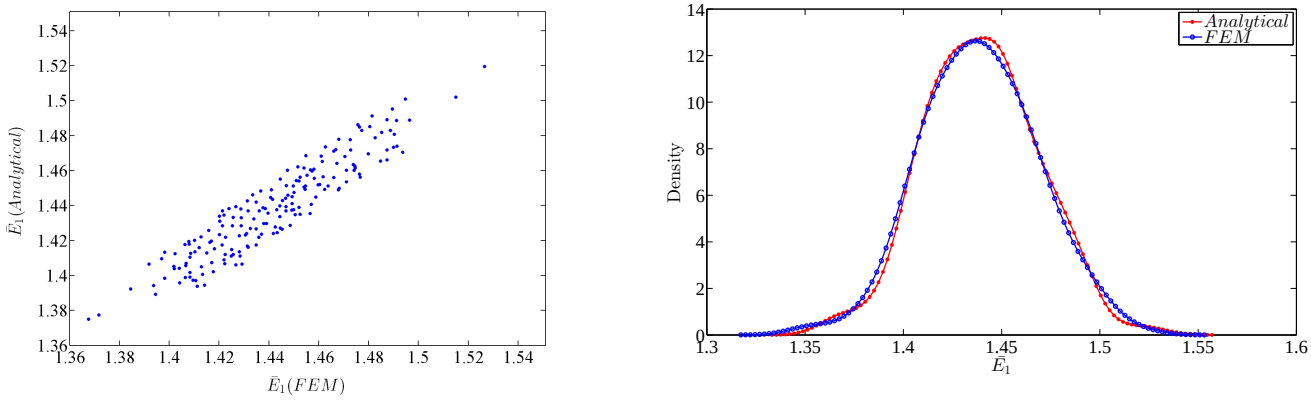


(a) Scatter plot

(b) Probability density function plot

Figure 12: Representative scatter plot and probability density function plot for $E_1$ considering a hexagonal configuration with $\theta = 30°$, $h/l = 1$ and $r = 8$.

values. On the other hand, the probability function plots furnished in figure 11(b) show that the standard deviation for relative density increases with the increase in cell angle ($\theta$).

Figure 12(a) shows a representative scatter plot for $E_1$, wherein low deviation of the points corresponding to different samples from the diagonal line affirms high level of precision of the developed analytical formulae with respect to finite element results for the irregular lattices. The low deviation between results of the probability density function plots presented in figure 12(b) using the analytical formulae and finite element method for $E_1$ of irregular lattice further corroborates high level of accuracy of the proposed approach. It is interesting to note that even though the nodes of the lattices corresponding to regular configuration are allowed to move within a circular bound following a random uniform distribution for obtaining the irregular lattice configurations, the effective $E_1$ of irregular lattice follows a Gaussian distribution. A similar trend is found in the results for other in-plane elastic moduli presented later (figure 13 - 27). This observation agrees well with the central limit theorem of probability theory (Rice, 1995).

The effect of irregularity on the five in-plane elastic moduli are presented in figures 13 -27 considering different degree of irregularity ($r$). The numerical values furnished in the left side of each '**I**' shaped marks represent percentage errors in mean values of in-plane elastic moduli obtained using the developed analytical formulae with respect to the finite element results, while the numerical values on top and bottom are the percentage errors corresponding to maximum and minimum values respectively. Reasonably small values in the percentage errors is indicative of high precision of the proposed analytical approach for irregular lattices compared to finite element formulation. The probabilistic description of the in-plane elastic moduli corresponding to different lattice configurations are shown

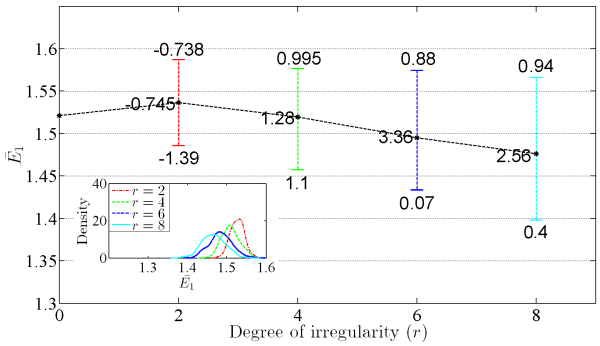


(a) $h/l = 1$

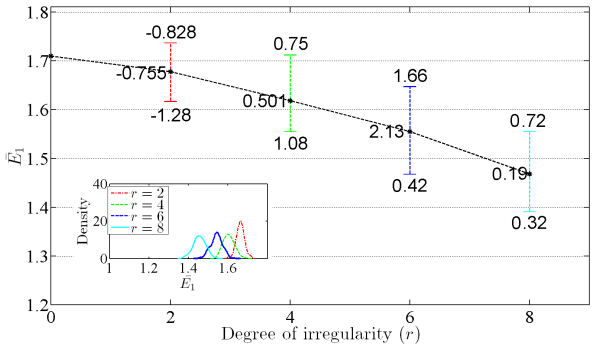


(b) $h/l = 1.5$

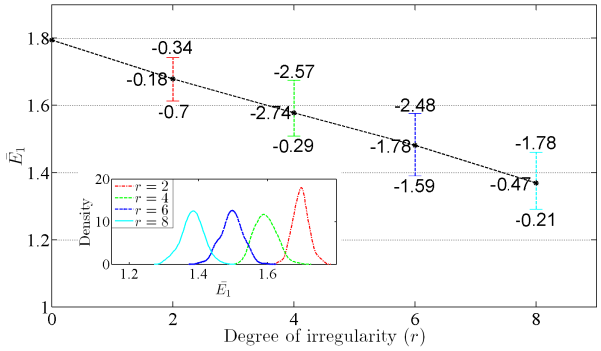


(c) $h/l = 2$

Figure 13: Effect of spatially random structural irregularity on non-dimensional $E_1$ for $\theta = 30°$

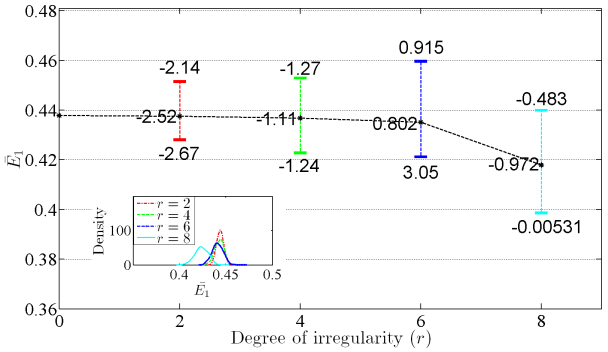


(a) $h/l = 1$

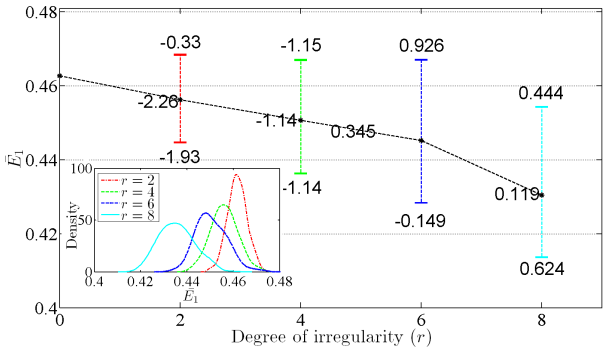


(b) $h/l = 1.5$

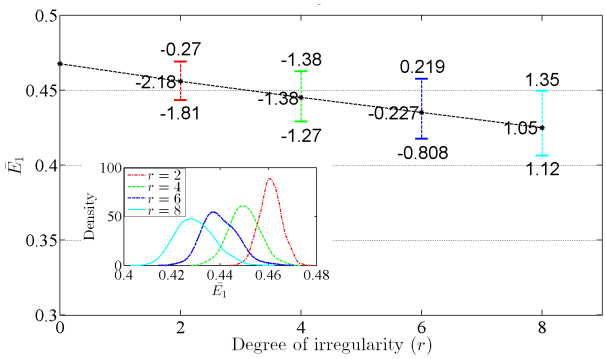


(c) $h/l = 2$

Figure 14: Effect of spatially random structural irregularity on non-dimensional $E_1$ for $\theta = 45°$

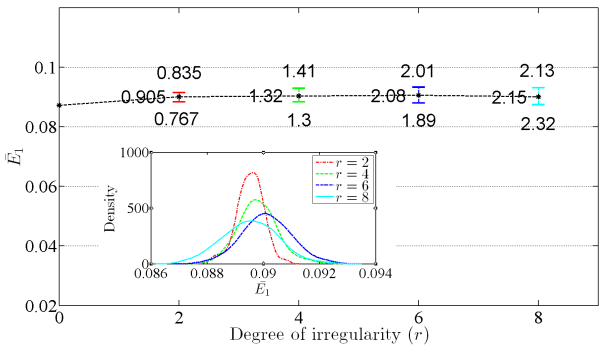


(a) $h/l = 1$

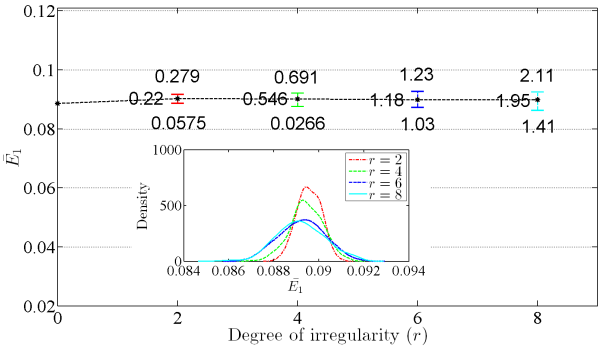


(b) $h/l = 1.5$

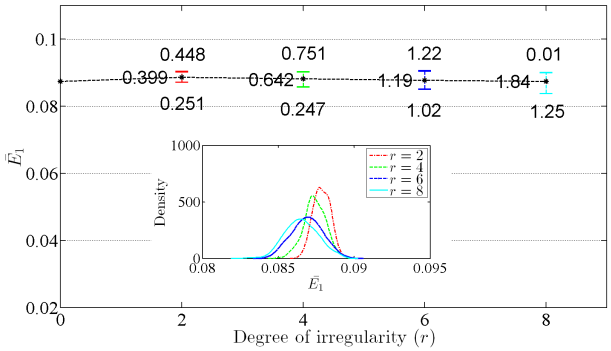


(c) $h/l = 2$

Figure 15: Effect of spatially random structural irregularity on non-dimensional $E_1$ for $\theta = 60°$

as inset of each figure.

From figures 13 - 27, it can be observed that the mean values of the two Young's moduli ($E_1$ and $E_2$) and two Poisson's ratios ($\nu_{12}$ and $\nu_{21}$) reduce with the increase in degree of irregularity, while the shear modulus ($G_{12}$) is found to follow an increasing trend with higher degree of irregularity. However, the upper bound for $E_1$ and the lower bound for $G_{12}$ are found to be respectively more and less than the corresponding deterministic values, in some instances due to system randomness depending on the respective standard deviations. The range of variations for all the in-plane elastic moduli are found to increase with increasing degree of irregularity, as expected. From relative slope of the lines joining mean values, it is observed that the effect of irregularity is more sensitive for increasing value of deterministic cell angle ($\theta$) in case of two Young's moduli ($E_1$ and $E_2$) and two Poisson's ratios ($\nu_{12}$ and $\nu_{21}$), while a reverse trend is found for the shear modulus ($G_{12}$). However, all the in-plane elastic moduli are found to be more sensitive to structural irregularity as the $h/l$ ratio decreases. From the results presented in figures 13 - 27, it is quite evident that the effect of spatially random structural irregularity has considerable influence on the equivalent in-plane elastic properties of hexagonal lattices (percentage variation are up to 27.22% and 13.41% for $E_1$ and $E_2$; 10.05% for

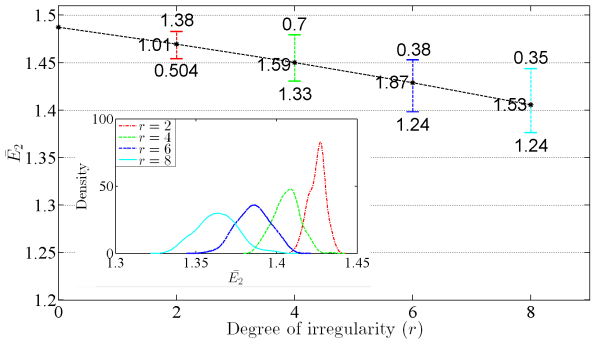


(a) $h/l = 1$

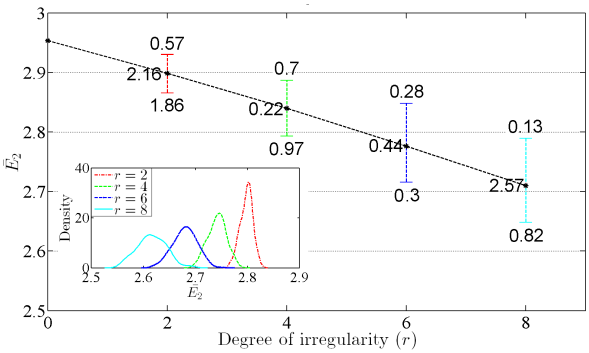


(b) $h/l = 1.5$

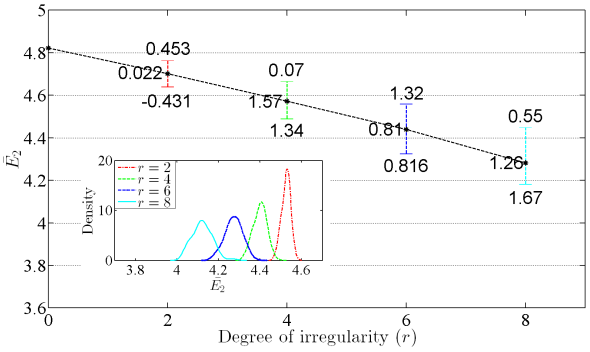


(c) $h/l = 2$

Figure 16: Effect of spatially random structural irregularity on non-dimensional $E_2$ for $\theta = 30°$

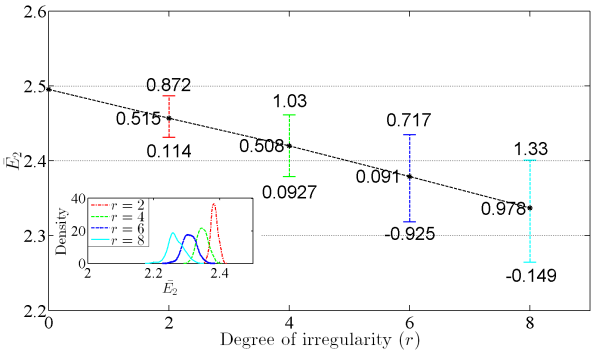


(a) $h/l = 1$

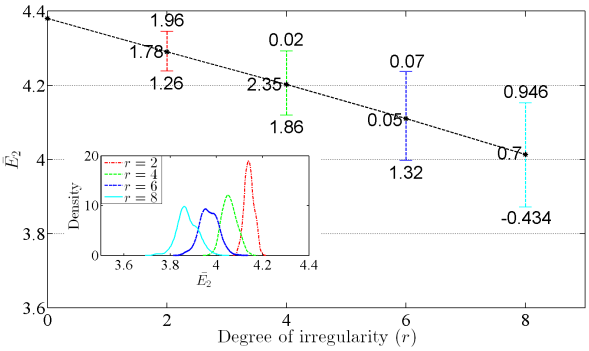


(b) $h/l = 1.5$

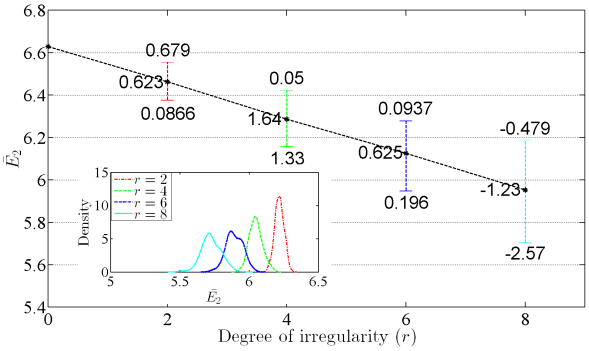


(c) $h/l = 2$

Figure 17: Effect of spatially random structural irregularity on non-dimensional $E_2$ for $\theta = 45°$

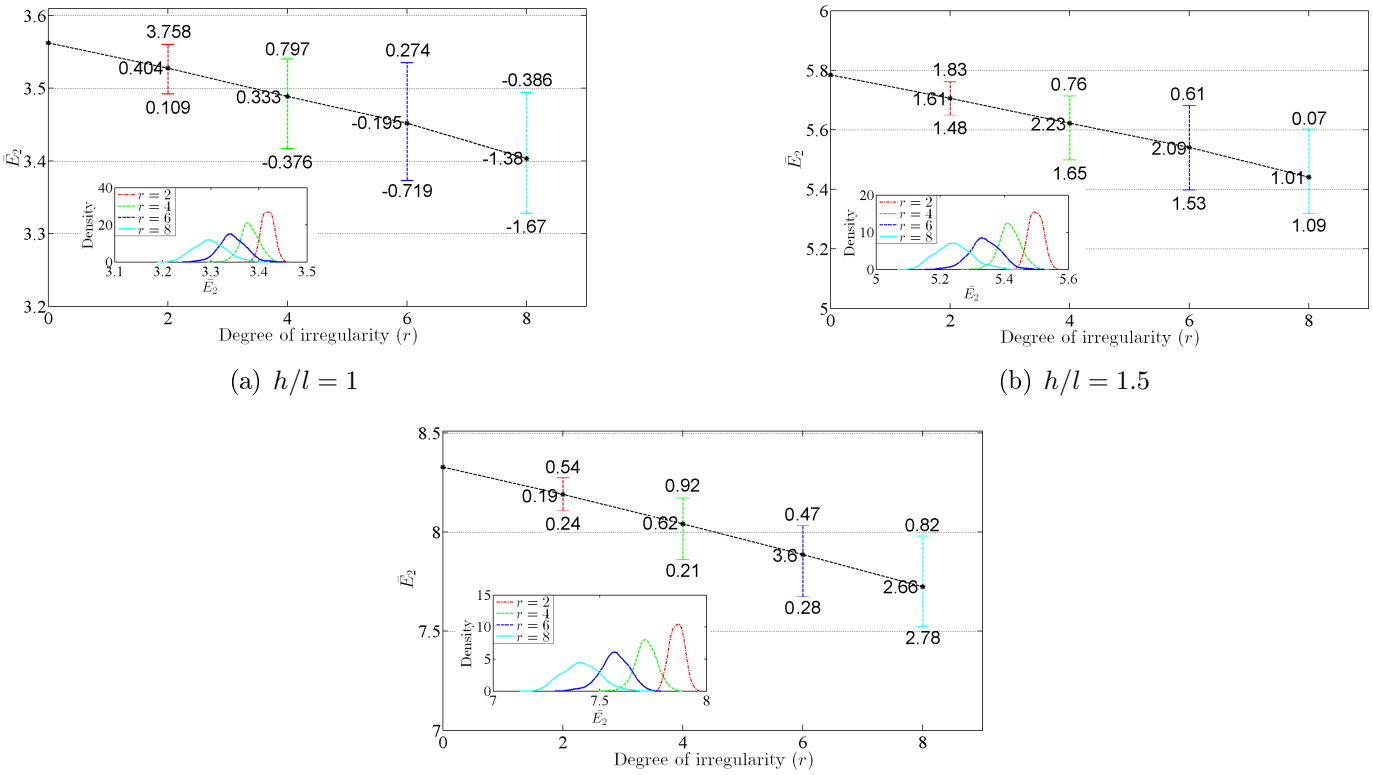


(a) $h/l = 1$

(b) $h/l = 1.5$

(c) $h/l = 2$

Figure 18: Effect of spatially random structural irregularity on non-dimensional $E_2$ for $\theta = 60°$

$G_{12}$; 28.43% and 21.18% for $\nu_{12}$ and $\nu_{21}$, respectively in case of the analysed lattice configurations). The overlapping zones of the probability density function plots for different degree of irregularity corresponding to a particular deterministic structural configuration depends on the sensitivity of the elastic modulus under consideration to structural irregularity and the respective standard deviation.

Probabilistic results concerning the spatially random variation of intrinsic material property and the compound effect of material and structural variation are provided in figure 28 and figure 29, respectively. The extent of the effect arising due to irregularity (both in terms of variation of intrinsic material property and structural geometry) can be easily discerned from the probabilistic descriptions. Two different degree of randomness in the material properties ($\Delta_m$) are considered in terms of percentage spatial variation for obtaining the results. The effect on the in-plane elastic moduli for combined spatially random variation of intrinsic material property ($\Delta_m$) and structural geometry ($r$) are shown in figure 29 considering different degree of irregularity in random material property distribution and structural configuration. Even though the response bounds of the elastic moduli are found to increase with increasing degree of randomness in intrinsic material property distribution, the effect of variation in material properties is less significant compared to the spatially random variation in structural

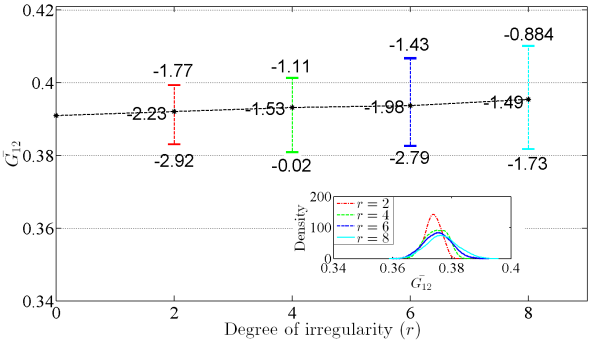


(a) $h/l = 1$

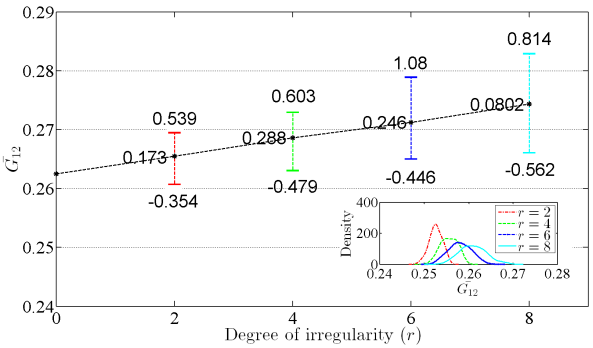


(b) $h/l = 1.5$

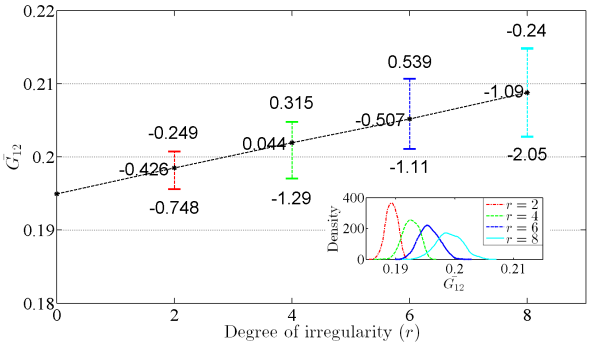


(c) $h/l = 2$

Figure 19: Effect of spatially random structural irregularity on non-dimensional $G_{12}$ for $\theta = 30°$

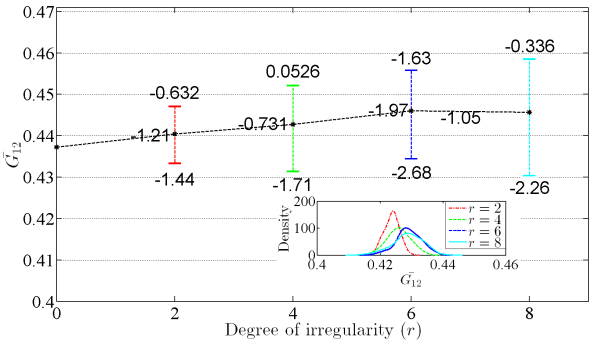


(a) $h/l = 1$

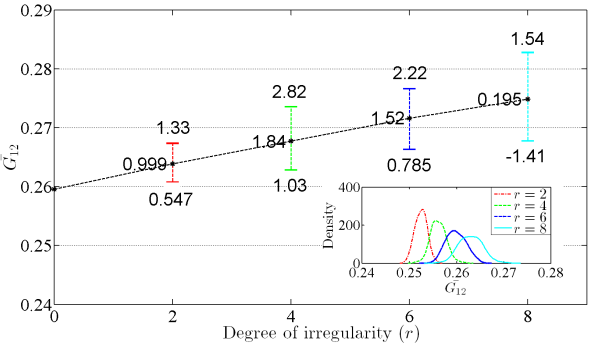


(b) $h/l = 1.5$

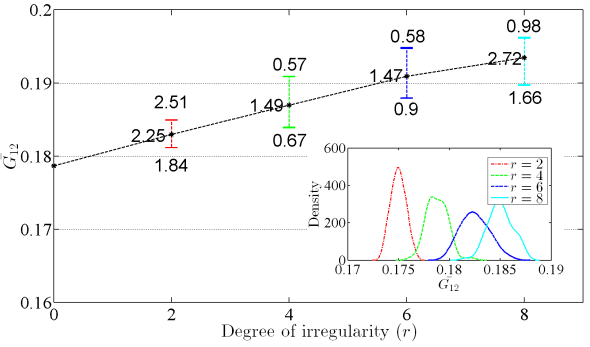


(c) $h/l = 2$

Figure 20: Effect of spatially random structural irregularity on non-dimensional $G_{12}$ for $\theta = 45°$

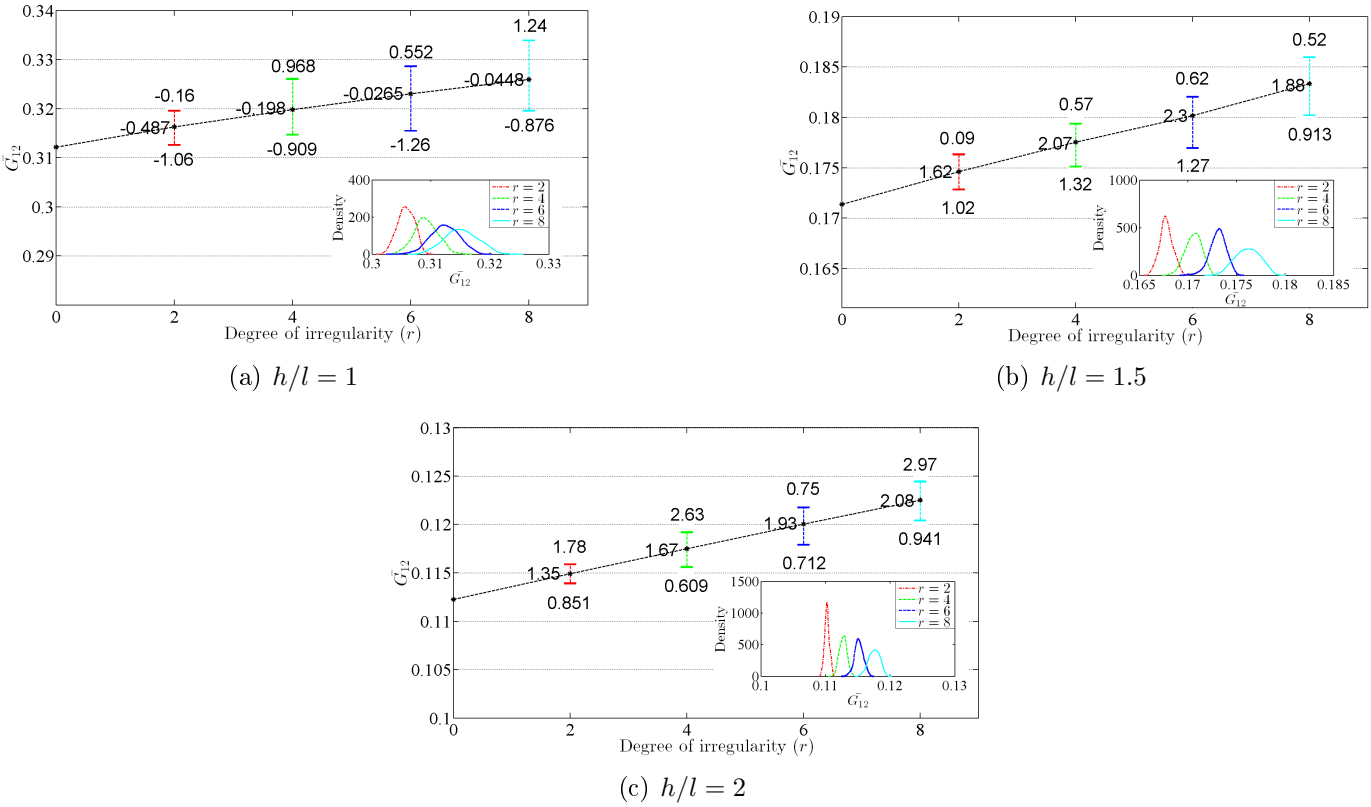


(a) $h/l = 1$ (b) $h/l = 1.5$

(c) $h/l = 2$

Figure 21: Effect of spatially random structural irregularity on non-dimensional $G_{12}$ for $\theta = 60°$

geometries. Similar inference can be drawn by comparing the probability distributions of in-plane elastic moduli for only variation of structural geometry and the compound effect of structural and material property variation as presented in figure 29. As the influence of the variability in structural configuration is quite significant compared to the spatial variability in intrinsic material property, the response bounds for the individual variation of structural configuration and the combined variation of structural and material property distribution do not have notable difference. However, the effect of intrinsic material property variation is found to be relatively more accountable in case of the shear modulus as the influence of structural irregularity is relatively lesser for the shear modulus compared to the Young's moduli.

Typical movement of nodes for regular lattices under the application of three different stress conditions (as described in figure 4) with two levels are shown in figure 30. Location of nodes for the deformed lattices can be visualized relative to respective undeformed configuration in the figures. Due to the cumulative effect, deflection of nodes for a particular level and condition of stress are higher as the distance from support increases. Movement of the nodes are higher in respective directions for stress level 2 compared to level 1, as expected. It is interesting to notice that the deformed location

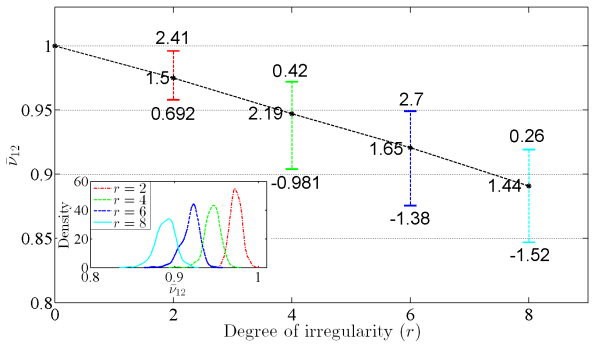


(a) $h/l = 1$

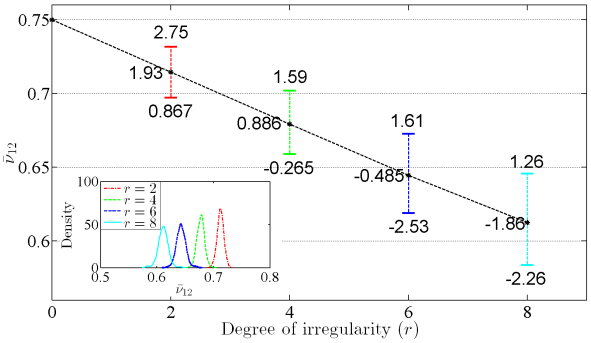


(b) $h/l = 1.5$

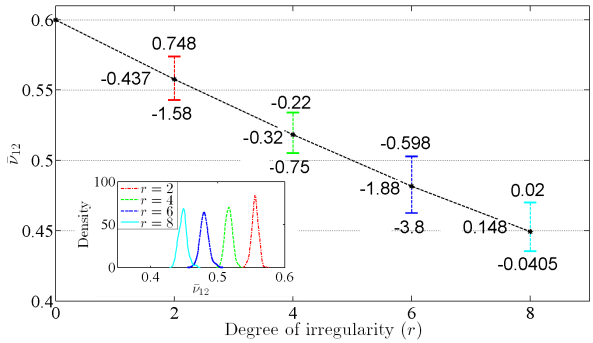


(c) $h/l = 2$

Figure 22: Effect of spatially random structural irregularity on non-dimensional $\nu_{12}$ for $\theta = 30°$

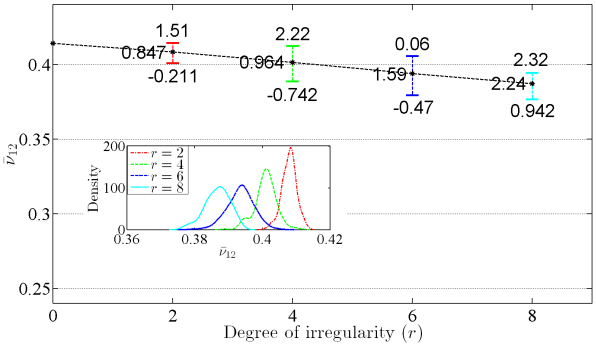


(a) $h/l = 1$

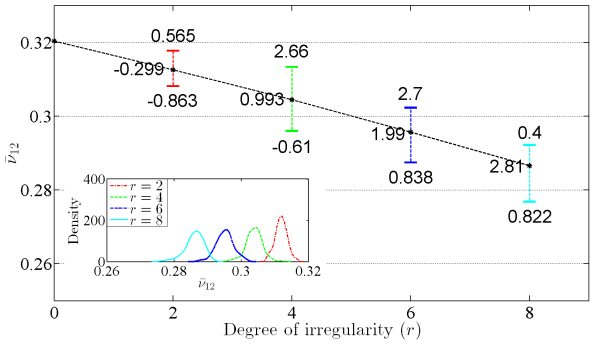


(b) $h/l = 1.5$

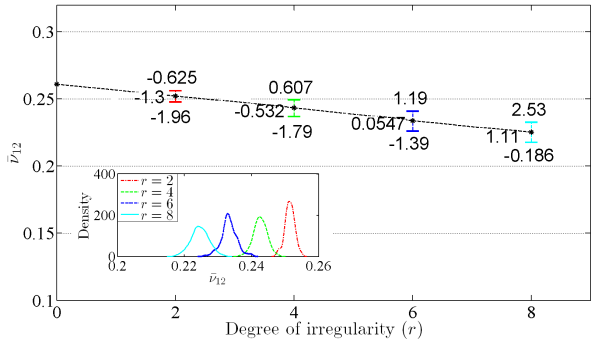


(c) $h/l = 2$

Figure 23: Effect of spatially random structural irregularity on non-dimensional $\nu_{12}$ for $\theta = 45°$

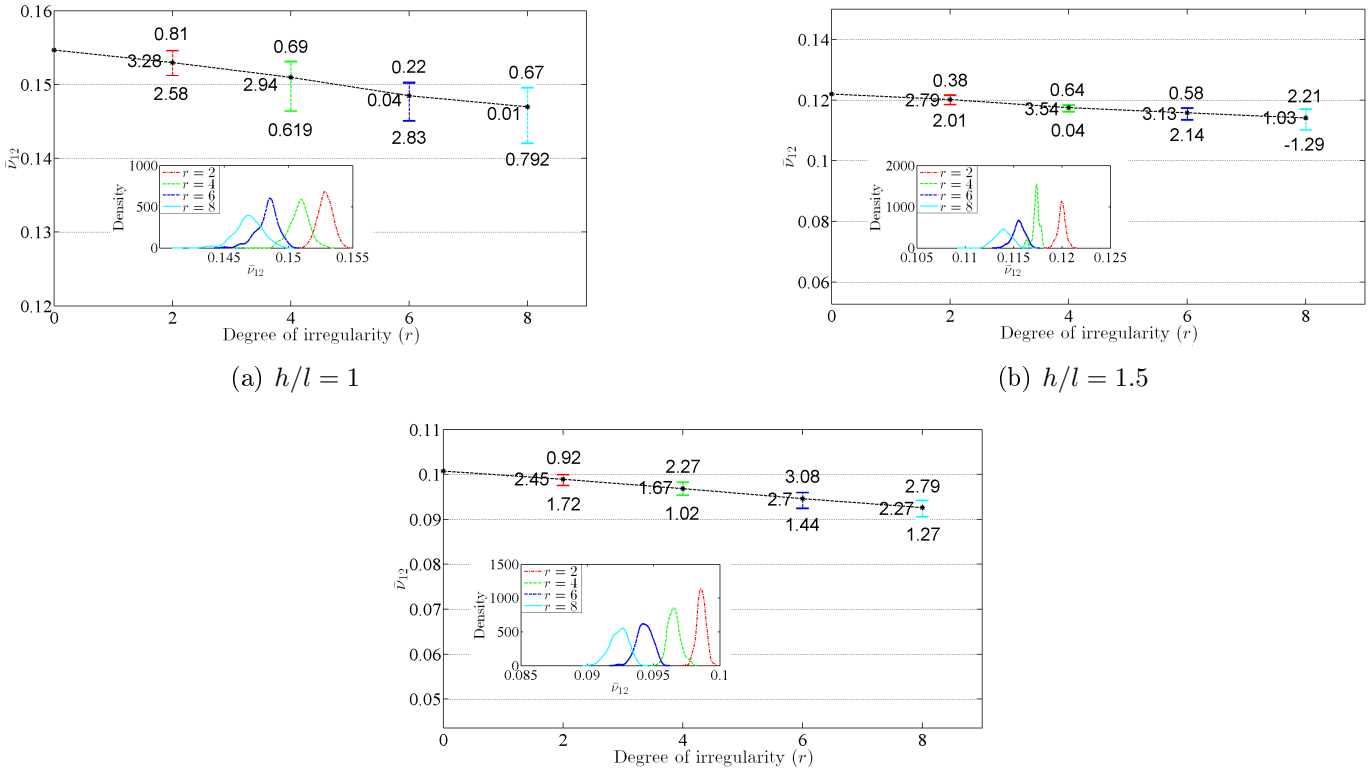


(a) $h/l = 1$ (b) $h/l = 1.5$

(c) $h/l = 2$

Figure 24: Effect of spatially random structural irregularity on non-dimensional $\nu_{12}$ for $\theta = 60°$

of the nodes for the stresses applied in direction-1 and direction-2 (figure 4(a) and 4(b)) allow the lattice to expand in the direction of applied stress while contract in the direction perpendicular to application of stress in the 1-2 plane, conforming non-auxetic property of the considered lattice configuration. If the cell angle corresponding to deterministic configurations ($\theta$) is considered negative, a reverse trend (expansion/contraction for both the directions) would be followed. Figure 31 shows typical irregular lattices for different random configurations along with location of nodes under the application of three different stress conditions. Figure 31(a), 31(c) and 31(e) present the movement of nodes for three different stress conditions considering a single random realization with structural irregularity, while figure 31(b), 31(d) and 31(f) show the bound of movements for different nodes and the connecting members in randomly irregular lattices in an ensemble form considering 10,000 random structural configurations. It is noteworthy that movement of the nodes in direction-1 and direction-2 (refer figure 31(a) - 31(d)) increases for randomly irregular structural geometries compared to the respective regular configurations, while for the application of shear stress (refer figure 31(e) - 31(f)), an opposite trend is noticed. This observation, in turn indicates reduction in $E_1$ and $E_2$ values of the lattice owing to effect of irregularity, while an increase in the value for $G_{12}$. Thus the results in

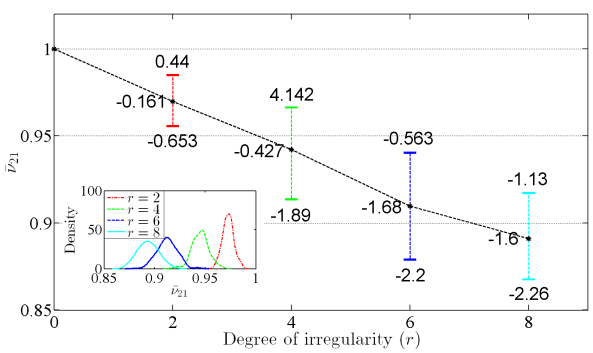


(a) $h/l = 1$

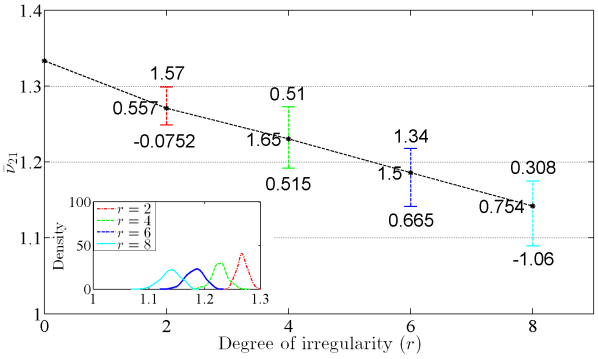


(b) $h/l = 1.5$

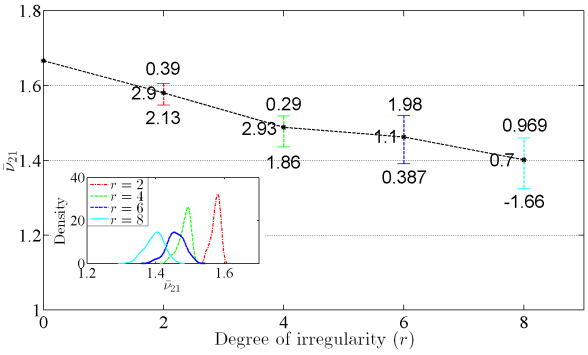


(c) $h/l = 2$

Figure 25: Effect of spatially random structural irregularity on non-dimensional $\nu_{21}$ for $\theta = 30°$

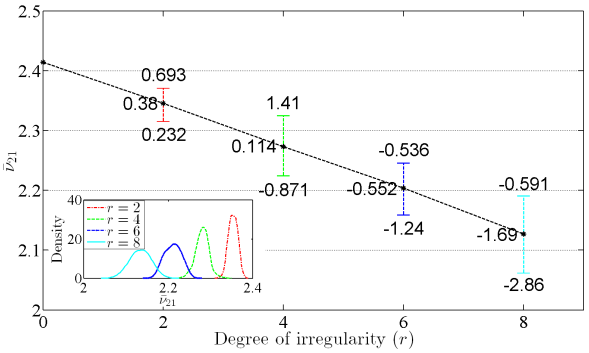


(a) $h/l = 1$

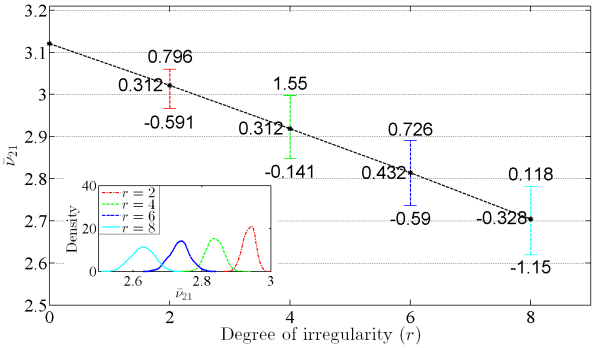


(b) $h/l = 1.5$

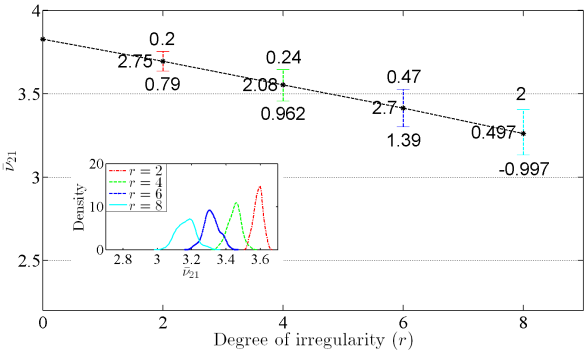


(c) $h/l = 2$

Figure 26: Effect of spatially random structural irregularity on non-dimensional $\nu_{21}$ for $\theta = 45°$

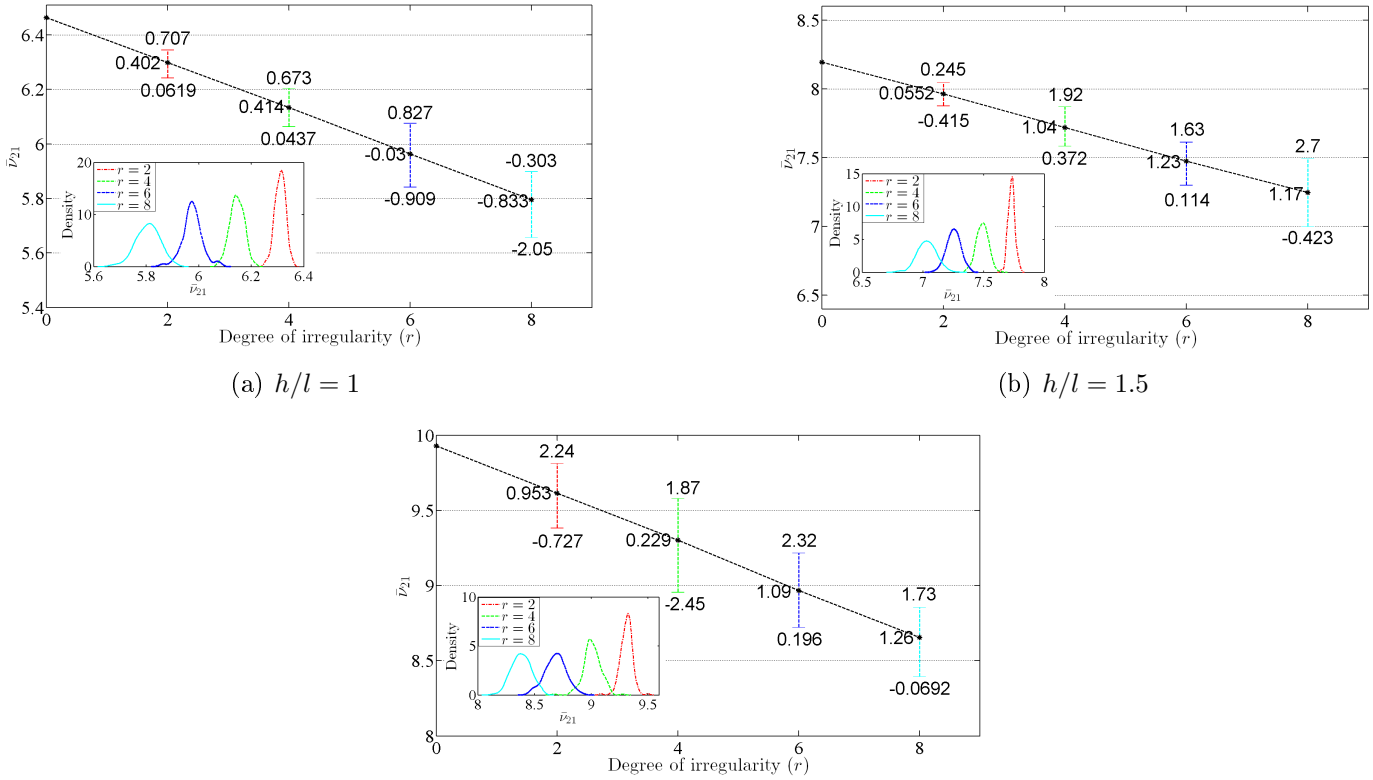


(a) $h/l = 1$ (b) $h/l = 1.5$

(c) $h/l = 2$

Figure 27: Effect of spatially random structural irregularity on non-dimensional $\nu_{21}$ for $\theta = 60°$

figure 31 agree well with the results presented in figures 13 - 21.

## 5. Summary and perspective

A careful review of the scientific literature reveals that previous investigations have dealt with the effect of under and over-expansion of cells in hexagonal honeycomb with regular configuration using numerical and experimental studies (Papka and Kyriakides, 1994) concluding that under-expansion results in a response that has a higher elastic moduli, while over-expansion has the opposite effect. The effect of spatially random variation of under and over expanded cells (refer to figure 2(b)) on the in-plane elastic moduli for irregular honeycombs are presented recently (Mukhopadhyay and Adhikari, 2016a,b), which reveal that $E_2$, $\nu_{21}$ and $G_{12}$ reduce significantly due to such variations in cell angle, while the effect on $E_1$ and $\nu_{12}$ is negligible. Liu et al. (2014) have reported, based on numerical investigation, that irregularity in auxetic hexagonal honeycombs reduces the effective in-plane Young's moduli and auxetic property of the system. The present paper develops an analytical framework to obtain effective in-plane elastic moduli of hexagonal lattices with a generalized form of random structural irregularity. The previous works (Mukhopadhyay and Adhikari, 2016a,b) on the development

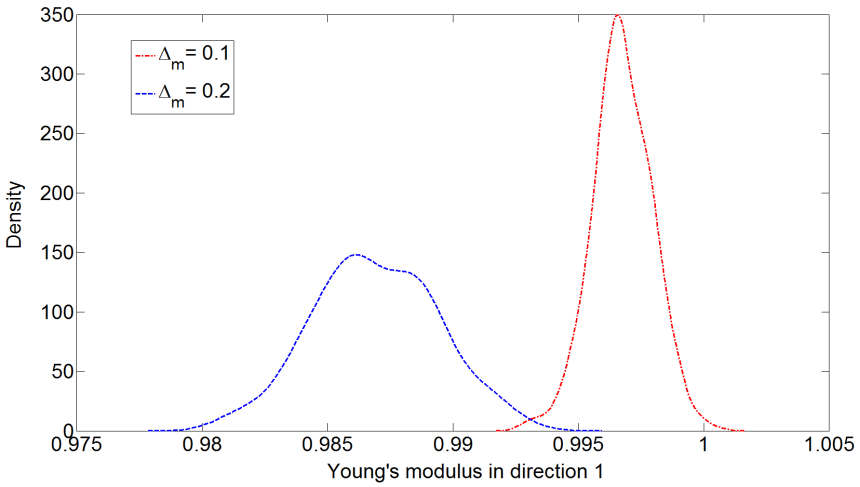


(a) Normalized longitudinal Young's modulus

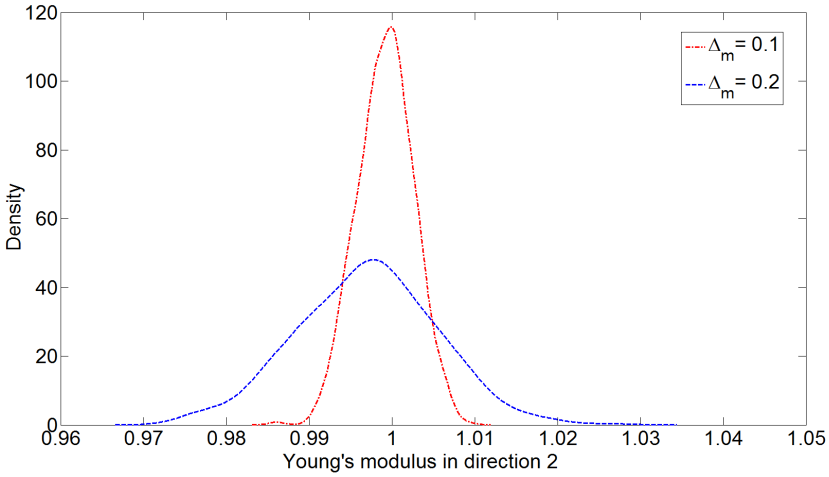


(b) Normalized transverse Young's modulus

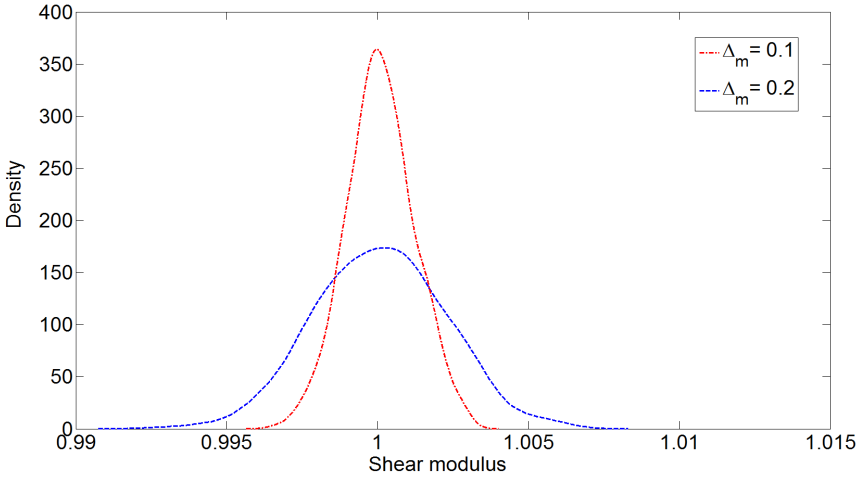


(c) Normalized shear modulus

Figure 28: Effect on the in-plane elastic moduli (probabilistic descriptions) for spatially random variation of intrinsic material property only (the results are presented as a ratio of the elastic moduli for irregular lattice and that of the corresponding regular configuration)

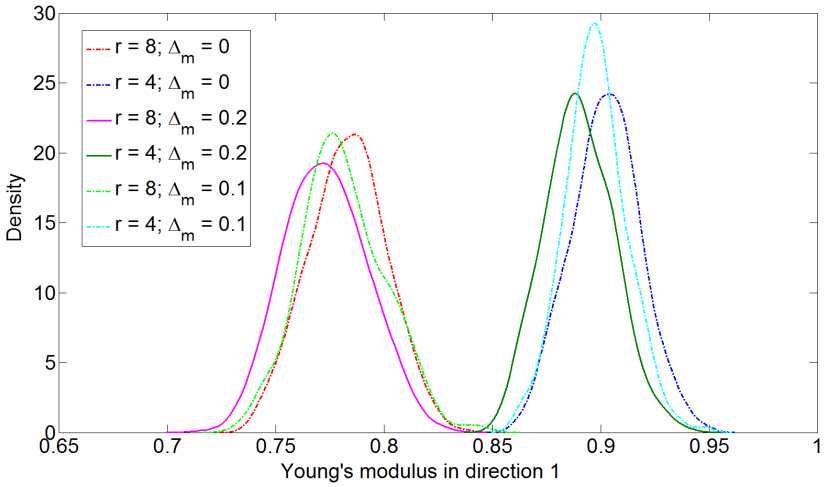


(a) Normalized longitudinal Young's modulus

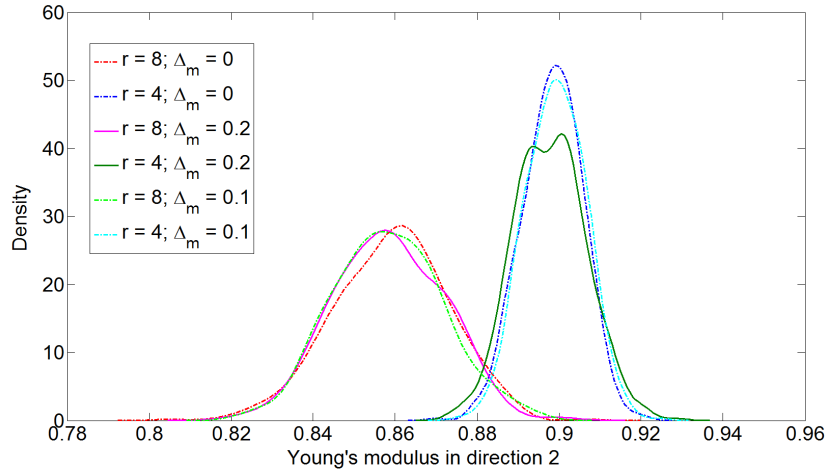


(b) Normalized transverse Young's modulus

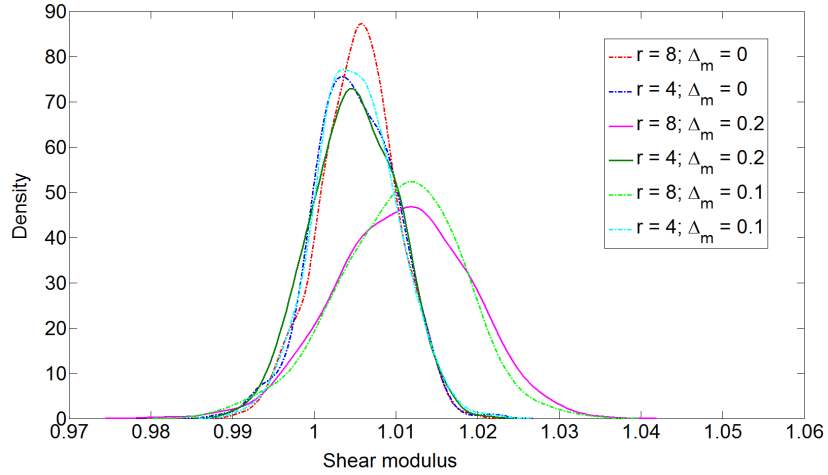


(c) Normalized shear modulus

Figure 29: Effect on the in-plane elastic moduli (probabilistic descriptions) for combined spatially random variation of intrinsic material property and structural geometry (the results are presented as a ratio of the elastic moduli for irregular lattice and that of the corresponding regular configuration)

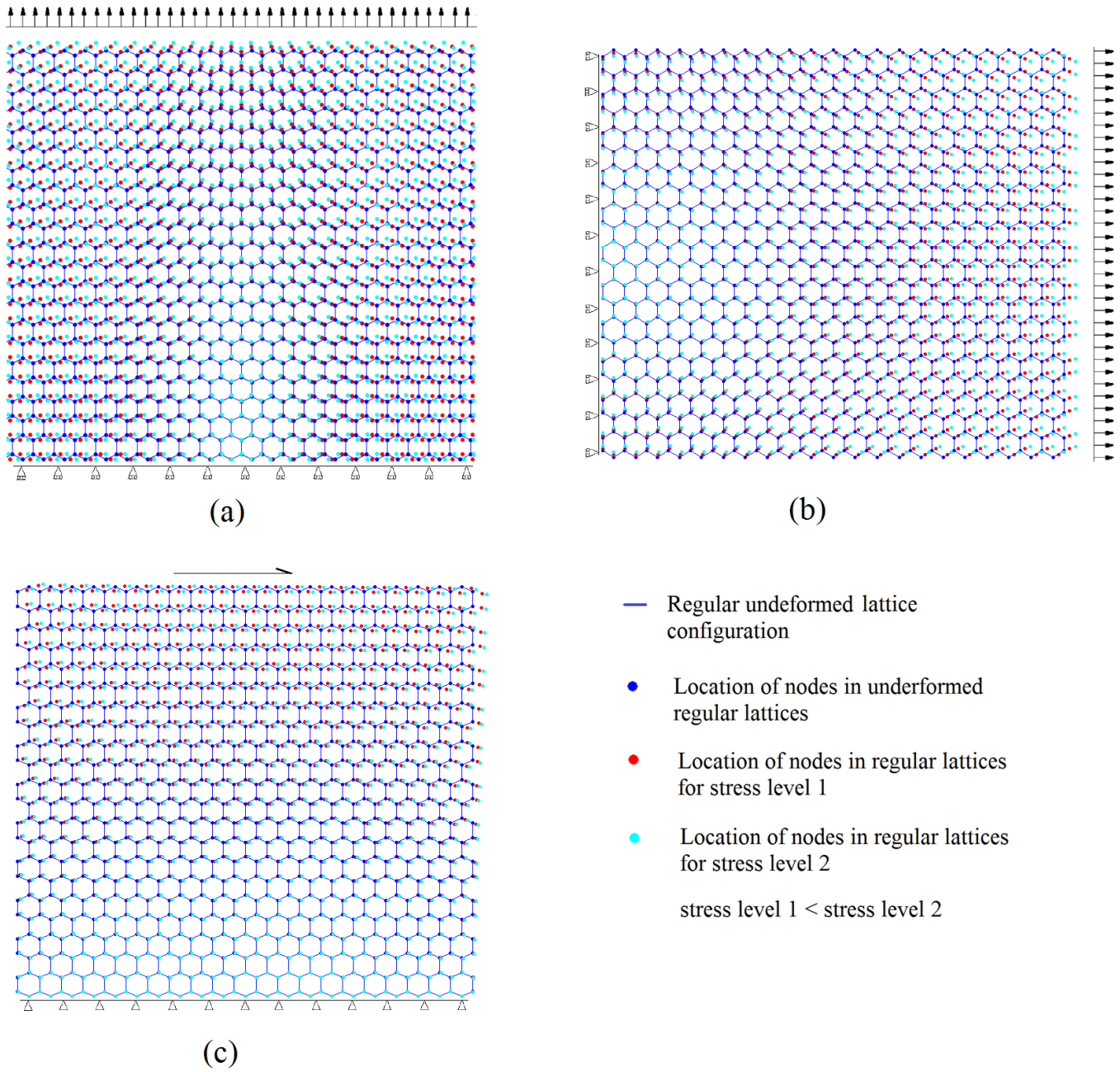


Figure 30: Typical location of nodes for a regular lattice under the application of three different stress conditions

of analytical formulae for randomly varying cell angles is a specialized case of the formulation presented here. In contrast to the previous observations related to spatially varying cell angles, the present study shows that all the in-plane elastic moduli are significantly affected by generalized randomness in structural configuration. The generalized form of spatially random irregularity, as considered in this study, results in decrease of mean for the two Young's moduli ($E_1$ and $E_2$) and two Poisson's ratios ($\nu_{12}$ and $\nu_{21}$), while an increase of mean for the shear modulus ($G_{12}$) is observed. The closed-form expressions developed for the two Young's moduli, and shear modulus are functions of both structural

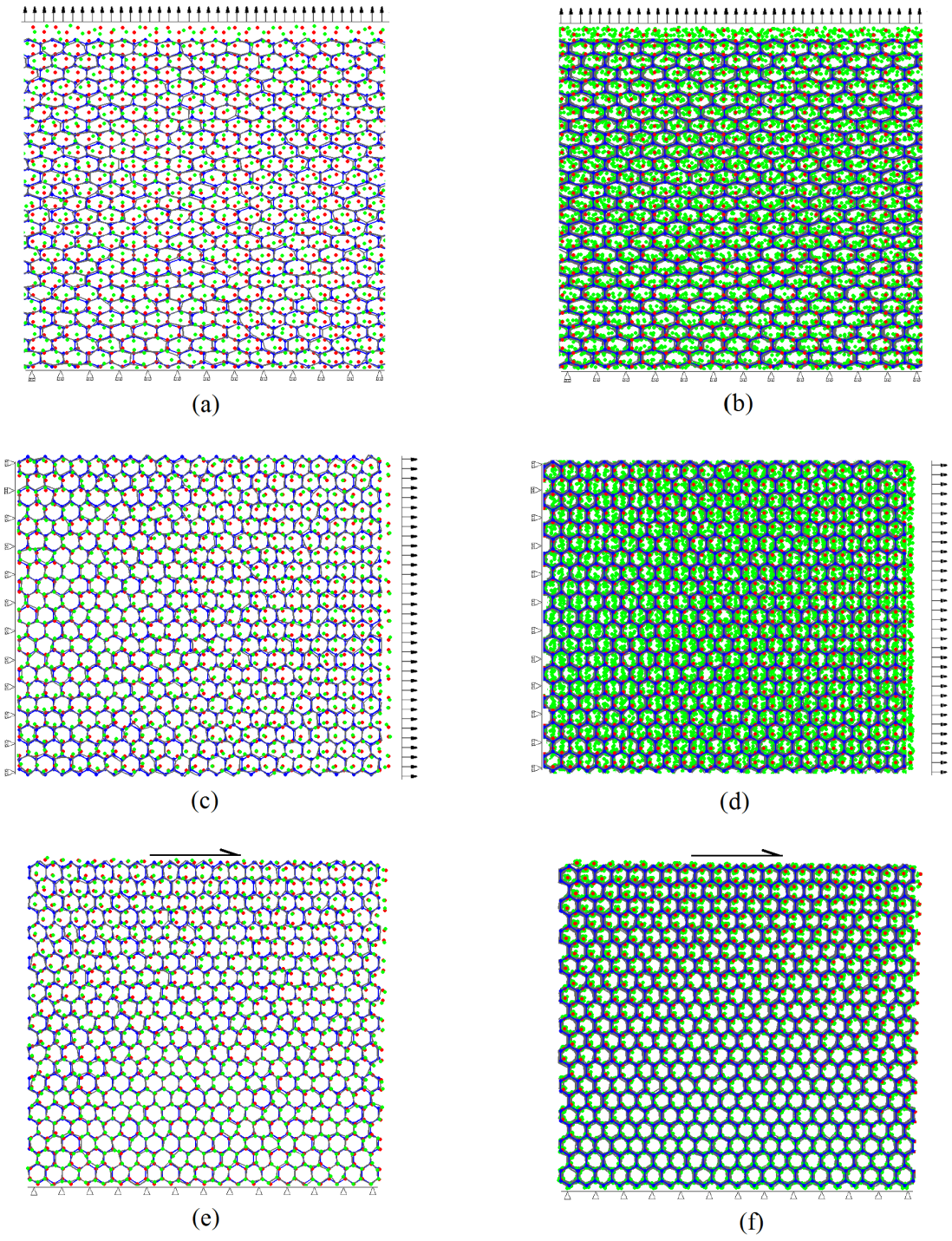


Figure 31: Typical representation for deformation of an irregular lattices along with location of nodes under the application of three different stress conditions

configuration and material properties of irregular lattice, while the two Poisson's ratios depend only on structural configuration. In addition to the other parameters the member with inclination angle $\gamma$ plays a vital role in variation of the elastic moduli for irregular lattices, as this member contributes towards the bending deformation significantly in the present analysis. Thus the form of irregularity in hexagonal lattices has considerable influence in the effective global behaviour (in-plane elastic properties) of the entire lattice. However, it is found that spatially random variation of intrinsic material property has less significant effect on the in-plane elastic moduli compared to the structural irregularity. Consideration of the shape of RUCE and adopted idealization scheme depends on the form of irregularity in the lattice. However, being the most generalized formulation, the present approach can account for all the above mentioned forms of irregularity.

Effect of different irregularities and defects in various forms of solids have received immense attention from the scientific community. Effect of material anisotropy on the effective elastic moduli has been investigated for solids (Sevostianov and Sabina, 2007; Tsukrov and Kachanov, 2000). Researchers have studied the effect of cracks in solids on the global behaviour such as effective elastic moduli, vibration etc. (Kachanov, 1987, 1992; Naskar et al., 2017) . The influence of such material anisotropy or defect in the form of multiple cracks on the effective elastic properties of solids are reported to be rather minimal. Though the configuration of lattice structures, as considered in this article, is quite different from these solids considered in the above-mentioned studies, we find a striking resemblance in the behaviour for variation of material properties. The effect of spatially random variation of intrinsic material property on the effective elastic moduli is found to be negligible compared to the structural randomness. This is because of an inherent averaging effect in the deformation of the randomized RUCEs with relatively lower and higher effective stiffness compared to their deterministic configuration. However, the spatially random variation of structural geometry can cause a significant change in the values of elastic moduli due to a change in the deformation mechanics of different members (percentage variation are up to 28.43% with respect to the deterministic values). In case of voronoi honeycombs, the elastic moduli have been reported to be significantly influenced (Zhu et al., 2001). Thus an important inference can be noted in this context that the influence of irregularity in a structural/ material system depends on their structural configuration and the type of irregularity under consideration.

Literature concerning different forms of irregularity in lattices as mentioned above are mostly based on either experimental investigation or numerical simulation. However, for characterizing the effect of random structural irregularity in lattice structures, it is essential to follow a probabilistic

framework requiring multiple numerical simulations/experiments. As detailed numerical simulations/ experiments are often expensive and time consuming, majority of the previously reported studies are performed based on an inadequate number of samples and semi-realistic irregularity models. Though an analytical approach has been recently reported (Mukhopadhyay and Adhikari, 2016b), that is limited to the variation of cell angles only. An efficient and realistic analytical framework capable of accounting generalized form of structural irregularity has been developed in the present paper including the effect of spatially varying structural configuration and intrinsic material property. Noteworthy is the fact that it has become possible to efficiently characterize the effect of structural irregularity including the probabilistic descriptions using a robust framework with adequate number of samples only because of development of the computationally efficient analytical approach.

## 6. Conclusion

A bottom-up analytical framework is developed for predicting equivalent in-plane elastic moduli of irregular hexagonal lattices having spatially random structural irregularity and intrinsic material property. In the proposed approach, effect of structural irregularities are accounted in the local level through representative unit cell elements (RUCE) first and thereby the effect of irregularity is propagated to the global level following a mechanics based multi-step approach to obtain effective in-plane properties of the entire irregular lattice. The results obtained using the developed analytical formulae for in-plane elastic moduli of irregular lattices are compared with the results from direct finite element simulations to establish the validity of the proposed approach. Noteworthy is the fact that equivalent in-plane elastic properties of irregular lattices can be obtained following a robust probabilistic framework using the closed-form formulae more efficiently compared to expensive finite element simulations (/experiment) without compromising the accuracy of results. All the in-plane elastic moduli are found to be affected significantly due to the consideration of spatially random structural configuration of lattices. Such variation in the elastic moduli of hexagonal lattices would have significant influence on the subsequent process of analysis, design and control.

Since the basic physics behind the elastic deformation of spatially irregular lattices is scale-independent, the developed closed-form formulae are applicable across different length scales. The developed formulae can be extended to predict effective in-plane elastic moduli of irregular lattices with spatial variation in the thickness of the connecting members. The analytical framework can be utilized for efficient stochastic analysis of such structures and material responses accounting the irregularity and uncertainty associated with spatial distribution of structural geometry and intrinsic material proper-

ties. Moreover, the generalized closed-form expressions accounting spatially varying structural configuration, thickness of connecting members and intrinsic material properties can be quite attractive in the development of novel meta-materials adopting a proper optimization algorithm to find the bespoke material micro-structure. The proposed analytical framework to analyse irregular hexagonal lattices can be extended further to other forms of cellular structures by considering an appropriate representative unit cell element.

**Acknowledgements**

TM acknowledges the financial support from Swansea University through the award of Zienkiewicz Scholarship. SA acknowledges the financial support from The Royal Society of London through the Wolfson Research Merit award.

**References**

Ajdari, A., Jahromi, B. H., Papadopoulos, J., Nayeb-Hashemi, H., Vaziri, A., 2012. Hierarchical honeycombs with tailorable properties. International Journal of Solids and Structures 49 (11-12), 1413 – 1419.

Ajdari, A., Nayeb-Hashemi, H., Canavan, P., Warner, G., 2008. Effect of defects on elastic-plastic behavior of cellular materials. Materials Science and Engineering: A 487 (1-2), 558 – 567.

Chen, D. H., Yang, L., 2011. Analysis of equivalent elastic modulus of asymmetrical honeycomb. Composite Structures 93 (2), 767–773.

Critchley, R., Corni, I., Wharton, J. A., Walsh, F. C., Wood, R. J. K., Stokes, K. R., 2013. A review of the manufacture, mechanical properties and potential applications of auxetic foams. Physica Status Solidi B 250 (10), 1963–1982.

Dey, S., Mukhopadhyay, T., Adhikari, S., 2017a. Metamodel based high-fidelity stochastic analysis of composite laminates: A concise review with critical comparative assessment. Composite Structures 171, 227 – 250.

Dey, S., Mukhopadhyay, T., Naskar, S., Dey, T., Chalak, H., Adhikari, S., 2017b. Probabilistic characterisation for dynamics and stability of laminated soft core sandwich plates. Journal of Sandwich Structures & Materials, DOI: 10.1177/1099636217694229.

Dey, S., Mukhopadhyay, T., Sahu, S., Adhikari, S., 2016a. Effect of cutout on stochastic natural frequency of composite curved panels. Composites Part B: Engineering 105, 188 – 202.

Dey, S., Mukhopadhyay, T., Spickenheuer, A., Adhikari, S., Heinrich, G., 2016b. Bottom up surrogate based approach for stochastic frequency response analysis of laminated composite plates. Composite Structures 140, 712 – 727.

Dey, S., Mukhopadhyay, T., Spickenheuer, A., Gohs, U., Adhikari, S., 2016c. Uncertainty quantification in natural frequency of composite plates: an artificial neural network based approach. Advanced Composites Letters 25, 43 – 48.

Dey, S., Naskar, S., Mukhopadhyay, T., Gohs, U., Spickenheuer, A., Bittrich, L., Sriramula, S., Adhikari, S., Heinrich, G., 2016d. Uncertain natural frequency analysis of composite plates including effect of noise – a polynomial neural network approach. Composite Structures 143, 130 – 142.

El-Sayed, F. K. A., Jones, R., Burgess, I. W., 1979. A theoretical approach to the deformation of honeycomb based composite materials. Composites 10 (4), 209–214.

Evans, K. E., Alderson, A., 2000. Auxetic materials: Functional materials and structures from lateral thinking! Advanced Materials 12 (9), 617–628.

Gibson, L., Ashby, M. F., 1999. Cellular Solids Structure and Properties. Cambridge University Press, Cambridge, UK.

Gonella, S., Ruzzene, M., 2008a. Analysis of in-plane wave propagation in hexagonal and re-entrant lattices. Journal of Sound and Vibration 312 (1 - 2), 125 – 139.

Gonella, S., Ruzzene, M., 2008b. Homogenization and equivalent in-plane properties of two-dimensional periodic lattices. International Journal of Solids and Structures 45 (10), 2897 – 2915.

Goswami, S., 2006. On the prediction of effective material properties of cellular hexagonal honeycomb core. Journal of Reinforced Plastics and Composites 25 (4), 393–405.

Hu, L. L., Yu, T. X., 2013. Mechanical behavior of hexagonal honeycombs under low-velocity impact-theory and simulations. International Journal of Solids and Structures 50 (20-21), 3152 – 3165.

Hurtado, J. E., Barbat, A. H., 1998. Monte carlo techniques in computational stochastic mechanics. Archives of Computational Methods in Engineering 5 (1), 3–29.

Jang, W. Y., Kyriakides, S., 2015. On the buckling and crushing of expanded honeycomb. International Journal of Mechanical Sciences 91, 81 – 90.

Javid, F., Liu, J., Shim, J., Weaver, J. C., Shanian, A., Bertoldi, K., 2016. Mechanics of instability-induced pattern transformations in elastomeric porous cylinders. Journal of the Mechanics and Physics of Solids 96, 1 – 17.

Jimenez, F. L., Triantafyllidis, N., 2013. Buckling of rectangular and hexagonal honeycomb under combined axial compression and transverse shear. International Journal of Solids and Structures

50 (24), 3934 – 3946.

Kachanov, M., 1987. Elastic solids with many cracks: A simple method of analysis. International Journal of Solids and Structures 23 (1), 23–43.

Kachanov, M., 1992. Effective elastic properties of cracked solids: critical review of some basic concepts. Appl. Mech. Rev 45 (8), 304–335.

Klintworth, J. W., Stronge, W. J., 1988. Elasto-plastic yield limits and deformation laws for transversely crushed honeycombs. International Journal of Mechanical Sciences 30 (3-4), 273 – 292.

Li, K., Gao, X. L., Subhash, G., 2005. Effects of cell shape and cell wall thickness variations on the elastic properties of two-dimensional cellular solids. International Journal of Solids and Structures 42 (5-6), 1777–1795.

Li, K., Gao, X. L., Wang, J., 2007. Dynamic crushing behavior of honeycomb structures with irregular cell shapes and non-uniform cell wall thickness. International Journal of Solids and Structures 44 (14-15), 5003 – 5026.

Liu, Q., Mo, Z., Wu, Y., Ma, J., Tsui, G. C. P., Hui, D., 2016. Crush response of cfrp square tube filled with aluminum honeycomb. Composites Part B: Engineering 98, 406 – 414.

Liu, W., Wang, N., Huang, J., Zhong, H., 2014. The effect of irregularity, residual convex units and stresses on the effective mechanical properties of 2d auxetic cellular structure. Materials Science and Engineering: A 609, 26–33.

Liu, Y., Xie, B., Zhang, Z., Zheng, Q., Xu, Z., 2012. Mechanical properties of graphene papers. Journal of the Mechanics and Physics of Solids 60 (4), 591–605.

Mahata, A., Mukhopadhyay, T., Adhikari, S., 2016. A polynomial chaos expansion based molecular dynamics study for probabilistic strength analysis of nano-twinned copper. Materials Research Express 3 (3), 036501.

Malek, S., Gibson, L., 2015. Effective elastic properties of periodic hexagonal honeycombs. Mechanics of Materials 91 (1), 226 – 240.

Michel, J., Moulinec, H., Suquet, P., 1999. Effective properties of composite materials with periodic microstructure: a computational approach. Computer Methods in Applied Mechanics and Engineering 172 (1), 109 –143.

Mousanezhad, D., Ebrahimi, H., Haghpanah, B., Ghosh, R., Ajdari, A., Hamouda, A. M. S., Vaziri, A., 2015. Spiderweb honeycombs. International Journal of Solids and Structures. doi: http://dx.doi.org/10.1016/j.ijsolstr.2015.03.036.

Mukhopadhyay, T., 2017. A multivariate adaptive regression splines based damage identification

methodology for web core composite bridges including the effect of noise. Journal of Sandwich Structures & Materials, DOI: 10.1177/1099636216682533.

Mukhopadhyay, T., Adhikari, S., 2016a. Effective in-plane elastic properties of auxetic honeycombs with spatial irregularity. Mechanics of Materials 95, 204 – 222.

Mukhopadhyay, T., Adhikari, S., 2016b. Equivalent in-plane elastic properties of irregular honeycombs: An analytical approach. International Journal of Solids and Structures 91, 169 – 184.

Mukhopadhyay, T., Adhikari, S., 2016c. Free vibration analysis of sandwich panels with randomly irregular honeycomb core. Journal of Engineering Mechanics 10.1061/(ASCE)EM.1943-7889.0001153 , 06016008.

Mukhopadhyay, T., Adhikari, S., 2017. Stochastic mechanics of metamaterials. Composite Structures 162, 85 – 97.

Mukhopadhyay, T., Dey, T. K., Chowdhury, R., Chakrabarti, A., Adhikari, S., 2015. Optimum design of frp bridge deck: an efficient rs-hdmr based approach. Structural and Multidisciplinary Optimization 52 (3), 459–477.

Mukhopadhyay, T., Mahata, A., Adhikari, S., Zaeem, M. A., 2016a. Effective elastic properties of two dimensional multiplanar hexagonal nano-structures. 2D Materials, DOI: 10.1088/2053-1583/aa551c.

Mukhopadhyay, T., Mahata, A., Dey, S., Adhikari, S., 2016b. Probabilistic analysis and design of hcp nanowires: An efficient surrogate based molecular dynamics simulation approach. Journal of Materials Science & Technology 32 (12), 1345 – 1351.

Mukhopadhyay, T., Naskar, S., Dey, S., Adhikari, S., 2016c. On quantifying the effect of noise in surrogate based stochastic free vibration analysis of laminated composite shallow shells. Composite Structures 140, 798 – 805.

Naskar, S., Mukhopadhyay, T., Sriramula, S., Adhikari, S., 2017. Stochastic natural frequency analysis of damaged thin-walled laminated composite beams with uncertainty in micromechanical properties. Composite Structures 160, 312 –334.

Pantano, A., Parks, D. M., Boyce, M. C., 2004. Mechanics of deformation of single- and multi-wall carbon nanotubes. Journal of the Mechanics and Physics of Solids 52 (4), 591–605.

Papka, S. D., Kyriakides, S., 1994. In-plane compressive response and crushing of honeycomb. Journal of the Mechanics and Physics of Solids 42 (10), 1499 – 1532.

Papka, S. D., Kyriakides, S., 1998. Experiments and full-scale numerical simulations of in-plane crushing of a honeycomb. Acta Materialia 46 (8), 2765 – 2776.

Rice, J. A., 1995. Mathematical Statistics and Data Analysis. Duxbury Press.

Roark, R. J., Young, W. C., 1976. Formulas for Stress and Strain. McGraw-Hill Book Company.

Schaeffer, M., Ruzzene, M., 2015. Wave propagation in multistable magneto-elastic lattices. International Journal of Solids and Structures 56-57, 78 – 95.

Sevostianov, I., Sabina, F. J., 2007. Cross-property connections for fiber reinforced piezoelectric materials with anisotropic constituents. International Journal of Engineering Science 45 (9), 719 – –735.

Srivastava, A., 2016. Metamaterial properties of periodic laminates. Journal of the Mechanics and Physics of Solids 96, 252 – 263.

Tang, T., Felicelli, S. D., 2015. Micromechanical models for time-dependent multiphysics responses of polymer matrix smart composites. International Journal of Engineering Science 94, 164 –180.

Triantafyllidis, N., Schraad, M. W., 1998. Onset of failure in aluminum honeycombs under general in-plane loading. Journal of the Mechanics and Physics of Solids 46 (6), 1089 – 1124.

Tsukrov, I., Kachanov, M., 2000. Effective moduli of an anisotropic material with elliptical holes of arbitrary orientational distribution. International Journal of Solids and Structures 37 (41), 5919 – 5941.

Vilchevskaya, E., Sevostianov, I., 2015. Effective elastic properties of a particulate composite with transversely-isotropic matrix. International Journal of Engineering Science 94, 139 – 149.

Wilbert, A., Jang, W. Y., Kyriakides, S., Floccari, J. F., 2011. Buckling and progressive crushing of laterally loaded honeycomb. International Journal of Solids and Structures 48 (5), 803 – 816.

Yongqiang, L., Zhiqiang, J., 2008. Free flexural vibration analysis of symmetric rectangular honeycomb panels with scsc edge supports. Composite Structures 83 (2), 154–158.

Zenkert, D., 1995. An Introduction to Sandwich Construction. Chameleon Press, London.

Zhang, J., Ashby, M. F., 1992. The out-of-plane properties of honeycombs. International Journal of Mechanical Sciences 34 (6), 475 – 489.

Zhu, H. X., Hobdell, J. R., Miller, W., Windle, A. H., 2001. Effects of cell irregularity on the elastic properties of 2d voronoi honeycombs. Journal of the Mechanics and Physics of Solids 49 (4), 857–870.

Zhu, H. X., Thorpe, S. M., Windle, A. H., 2006. The effect of cell irregularity on the high strain compression of 2d voronoi honeycombs. International Journal of Solids and Structures 43 (5), 1061 – 1078.

Zschernack, C., Wadee, M. A., Vollmecke, C., 2016. Nonlinear buckling of fibre-reinforced unit cells of lattice materials. Composite Structures 136, 217 – 228.